2020

Energy, exergy and economic analyses of new coal-fired cogeneration hybrid plant with wind energy resource

Zhixiong Li
University of Wollongong, lizhixio@uow.edu.au

M Ehyaei

A Ahmadi

Dima Jamali

Ranjit Kumar
rkk376@uow.edu.au

See next page for additional authors

Energy, exergy and economic analyses of new coal-fired cogeneration hybrid plant with wind energy resource

Abstract

© 2020 Elsevier Ltd A novel configuration of a coal-fired cogeneration plant is proposed in this paper. This novel system is composed of combustion chamber, Rankine cycle, absorption chiller, alkaline electrolyzer, and methanation plant. In the proposed configuration, the heat of exhaust gas from the combustion chamber can be used in a Rankine cycle to produce electricity. The heat of exhaust gas also powers the absorption chiller to provide cooling. The exhaust gas flows through a sulfur extraction unit to separate sulfur from CO2 gas. To supply electrical power, wind turbines alongside the Rankine cycle are considered. A part of the produced electricity from both the Rankine cycle and the wind turbines can be used by an alkaline electrolyzer to produce hydrogen and oxygen. The CO2 gas from sulfur unit and hydrogen gas (H2) provided by the electrolyzer can be delivered to a methanation unit to produce syngas (CH4) for different applications. The oxygen from the electrolyzer is injected into the combustion chamber to improve the combustion process. Results show that by using 80 units of 1 MW Nordic wind turbine to generate electricity, all of the CO2 in the exhaust gas is converted to syngas. The whole system energy and exergy efficiencies are equal to 16.6% and 16.2%. The highest and lowest energy efficiencies of 85% and 30.1% are related to compressor and steam power plants. The energy and exergy efficiencies of the wind turbine are 30.7% and 11.9%. The system can produce 40920.4 MWh of electricity and 180.5 MWh of cooling. As CO2 is consumed to produce syngas, the proposed system is capable of avoiding a significant amount of 2776 t CO2 emissions while producing 1009.4 t syngas annually. Based on economic analysis, the payback period of the system is 11.2 y, and internal rate of return is found to be 10%, which can prove the viability of the proposed configuration.

Disciplines

Engineering | Science and Technology Studies

Publication Details

Li, Z., Ehyaei, M., Ahmadi, A., Jamali, D., Kumar, R. & Abanades, S. (2020). Energy, exergy and economic analyses of new coal-fired cogeneration hybrid plant with wind energy resource. Journal of Cleaner Production, 269

Authors

Zhixiong Li, M Ehyaei, A Ahmadi, Dima Jamali, Ranjit Kumar, and Stephane Abanades

Energy, exergy and economic analyses of new coal-fired cogeneration hybrid plant with wind energy resource

Z.X.Li[i(1), (2)], M.A. Ehyaei[(3)*], A. Ahmadi[(4)], D. H. Jamali[(5)], R. Kumar[(6)], Stéphane Abanades[(7)]

1. School of Engineering, Ocean University of China, Tsingdao 266100, China

2.School of Mechanical, Materials, Mechatronic and Biomedical Engineering, University of Wollongong, Wollongong, NSW 2522, Australia

3. Department of Mechanical Engineering, Pardis Branch, Islamic Azad University, Pardis New City, Iran

4. Iran University of Science and Technology, School of New Technologies, Department of Energy Systems Engineering, Iran

5. School of Environment, College of Engineering, University of Tehran, Tehran, Iran

6. School of Mechanical Engineering, Lovely Professional University, Phagwara, Punjab, India

7. Processes, Materials, and Solar Energy Laboratory, PROMES-CNRS, 7 Rue du Four Solaire, 66120 Font-Romeu, France

***Corresponding author: E-mail: aliehyaei@yahoo.com, Tel: +98-9123478028**

Abstract. A novel configuration of a coal-fired cogeneration plant is proposed in this paper. This novel system is composed of combustion chamber, Rankine cycle, absorption chiller, alkaline electrolyzer, and methanation plant. In the proposed configuration, the heat of exhaust gas from the combustion chamber can be used in a Rankine cycle to produce electricity. The heat of exhaust gas also powers the absorption chiller to provide cooling. The exhaust gas flows through a sulfur extraction unit to separate sulfur from CO_2 gas. To supply electrical power, wind turbines alongside the Rankine cycle are considered. A part of the produced electricity from both the Rankine cycle and the wind turbines can be used by an alkaline electrolyzer to produce hydrogen and oxygen. The CO_2 gas from sulfur unit and hydrogen gas (H_2) provided by the electrolyzer can be delivered to a methanation unit to produce syngas (CH_4) for different applications. The oxygen from the electrolyzer is injected into the combustion chamber to improve the combustion process. Results show that by using 80 units of 1 MW Nordic wind turbine to generate electricity, all of the CO_2 in the exhaust gas is converted to syngas. The whole system energy and exergy efficiencies are equal to 16.6% and 16.2%. The highest and lowest energy efficiencies of 85% and 30.1% are related to compressor and steam power plants. The energy and exergy efficiencies of the wind turbine are 30.7 % and 11.9 %. The system can produce 40920.4 MWh of electricity and 180.5 MWh of cooling. As CO_2 is consumed to produce syngas, the proposed system is capable of avoiding a significant amount of 2776 t CO_2 emissions while producing 1009.4 t syngas annually. Based on economic analysis, the payback period of the system is 11.2 y, and internal rate of return is found to be 10%, which can prove the viability of the proposed configuration.

Keywords: Energy, Exergy, Power to gas, Methanation, Rankine cycle, Wind turbine

1. Introduction

The worldwide energy demand for electricity generation is growing steadily. Fossil fuel is playing a major role to fulfill this demand. The excessive use of fossil fuel within the current energy infrastructure is causing natural disasters and health issues. The continuous CO_2 emissions are at least partially responsible for global warming (Atabi et al., 2014; Mozafari and Ehyaei, 2012). In 2016, coal-based power plants and other carbon-intensive sectors for electricity and heat generation contributed to 42% of global emissions (Shirmohammadi et al., 2018). By 2040, it is expected that global energy-related carbon dioxide emissions may reach around 43.2 billion t (Conti et al., 2016). These considerable global emissions are forcing policymakers to adopt an eco-friendly and sustainable alternative option for power generation in the entire world. Renewable Energy (RE) sources may play a key role to achieve this target because of their environmentally-friendly nature. Solar and wind energy resources are playing a crucial role in electricity generation while shifting fossil fuel consumption towards cleaner energy sources (Dorotić et al., 2019; Shaygan et al., 2019). According to an estimate, RE sources contribution to power supply was estimated to be more than 30% during 2010-2015 (Bellocchi et al., 2019). The impact of implementing RE sources in the heat and transportation sector is attracting more attention due to the dependency of this sector on fossil fuels (Dorotić et al., 2019). The European Commission target included 20% of RE contribution in its 2021 energy roadmap (Roadmap, 2011). Amongst various RE resources, the wind power promises a great potential in electricity generation and it reached up to 539 GW in 2017 globally. Hydrogen is also a promising viable option to replace fossil fuels for reliable power generation and for being used as vehicles fuel. The main advantage of hydrogen as an energy carrier is its flexible conversion into other energy forms in an efficient way in comparison to fossil fuels (Castaneda et al., 2013; Li et al., 2019).

Due to rapid growth in gas-fired based electricity generation, the integration of electricity, district heating and RE resources are attracting research towards clean energy generation in recent years. Researchers are also focusing on wind-solar hybrid power plants and trying to integrate different energy carriers in an energy hub (Gholizadeh et al., 2019; Yang et al., 2018). It has been proven that multi-products system can significantly enhance the performance of the system in comparison to single-product system (Jamali and Noorpoor, 2019; Li et al., 2019). The rules and regulations set by international organizations to mitigate climate changes are forcing the nations to promote clean energy (Lisbona et al., 2018).

The search for innovative technologies framework for sustainable development is getting more importance in the energy sector in recent years. Power-to-gas (PtG) technique is a viable option for the storage of surplus electricity generated by RE sources. It is a rising technology in the future energy sector to compete with existing technologies used for power generation (Walker et al., 2017; Weidner et al., 2018). In PtG, gas fuel is produced and long-term stored using electricity. The main advantage of this technology is that the surplus electricity is absorbed from the grid. Wind and solar power have great potential for the long term PtG operation (Guandalini et al., 2017). The use of an electrolyzer provides hydrogen from the electricity (Kreuter and Hofmann, 1998). There are various types of electrolysis technologies such as high-temperature electrolysis, alkaline water electrolysis, and polymer electrolyte electrolysis that are developed worldwide at large, laboratory and small scale (Buttler and Spliethoff, 2018). The separated pure hydrogen along with captured CO_2 can be used directly in the methanation process to produce Synthetic Natural Gas (SNG) (Ghaib and Ben-Fares, 2018). This gas can be used as a carbon-neutral fuel in the transport sector to reduce the level of CO_2 emissions. Another research was carried out to compare different catalysts usually used for CO_2 methanation. The catalysts were tested to determine the most suitable operating temperature and pressure, which turned out to be 673 K and 10 bar (García–García et al., 2018).

PtG systems proved to be suitable for sustainable energy storage using renewable energy sources (Lewandowska-Bernat and Desideri, 2018; Llera et al., 2018). Several studies on PtG plant have also been performed in recent years. PtG projects in Europe have been reviewed and discussed in detail (Wulf et al., 2018). PtG and Power to liquid (PtL) were identified as promising concepts to avoid source fluctuations when renewable energies are considered as primary energy sources. The CO_2 reduction trends were predicted in the case of using these technologies, and biomass gasification with subsequent hydrogenation could have great performance in integration with PtG systems (Bellocchi et al., 2019). Schaaf et al. (2014) proposed a system to store excess electricity produced from renewable sources such as solar and wind power plants and to use this electricity to provide hydrogen for the methanation with CO_2. In another study, a retrofit unit was integrated into a gas turbine plant for methanation purposes. In that system, the CO_2 was extracted from flue gas of the gas turbine plant, and hydrogen was provided from water electrolysis to produce methane (Boubenia et al., 2017). Direct methanation of flue gas was proposed using renewable hydrogen production by Laquaniello et al.(2018). The integration of hydrogen in PtG networks was assessed to find out its effect on the natural gas pipelines infrastructure (Gondal, 2019). A study focused on efficiency enhancement of a Sabatier-based PtG system by pinch analysis method, which revealed the significant potential of this concept. By thermoeconomic and sensitivity analysis, the critical components of the plant were highlighted (Toro and Sciubba, 2018). A system to integrate biogas plant to a membrane-based PtG system was also proposed. Two different processes for methanation were compared to study their feasibility (Kirchbacher et al., 2018). Applications of PtG were studied by retrofit plants in building energy systems through three different configurations (De Santoli et al., 2017). The impact of curtailment of wind-based generation on PtG was performed and the results showed that the impact of the activity was positive (Gholizadeh et al., 2019). A hybrid technology using PtG-biomass was reported to be most suitable in process industries (Bailera et al., 2016). Several studies have shown substantial cost reduction for methanation process and electrolysis, and this trend should continue until 2050 (Thema et al., 2019). Thermo-economic analysis of Sabatier based PtG plant was achieved to enhance plant efficiency (Toro and Sciubba, 2018). Thermodynamic, economic and environmental analyses were performed and showed promising results considering that water electrolysis will experience investment cost reduction (Boubenia et al., 2017). In another research, a 100 MW PtG was proposed and analyzed from an economic point of view, in which the system used solid oxide cell to both produce hydrogen and to use it reversibly for electricity generation when power is lacking (Miao and Chan, 2019). In a study, a gas turbine, an air bottoming cycle and a steam reforming unit were integrated for electricity and hydrogen production (Ahmadi et al., 2020). They found that adding steam reforming unit to the integrated gas and air bottoming cycles could enhance the energy and exergy efficiencies, and this combination would be advantagous from economic and environmental aspects.

The previous studies conclude that the utilization of carbon dioxide in syngas production is highly required because of the lower impact during combustion. In the present study, an integrated new system configuration using electricity from steam cycle and wind power plant along with gas through oxy-fuel combustion unit to produce syngas has been investigated. Thermal performance analysis of the plant has been performed in this study. The entire plant is a complex system due to the number of components working simultaneously in parallel and in series combination. This new system with such configuration has never been proposed so far. In this novel configuration, in the burner, coal is burned with air to produce hot gas. Hot gas energy is recovered in the Rankine cycle and absorption chiller to produce electricity and cooling. Sulfur components are removed from the exhaust gas and CO_2 is reacted with hydrogen in the methanation plant to produce syngas (CH_4). This syngas is pressurized with compressor and stored in the pressure vessel. The syngas produced at the outlet of the plant can be compressed and utilized for vehicles as a fuel. Energy and exergy analyses of individual components of the proposed plant have been proposed. The electrical power consumption of the system components matches the electricity produced by both the Rankine cycle and wind turbine. The novelties of this study are the proposal of an integrated new configuration of power to gas cycle with energy recovery of exhaust hot gas from the boiler. The reduction of a large portion of CO_2 emissions via conversion to syngas by using wind energy is an important aspect, which is highly desirable to reduce environmental pollution in present situation. Sensitivity analysis of the main parameters of this system is performed to evaluate the impact of several decision variables on the system performance.

2. Mathematical modeling

2.1. Process description

The schematic diagram of the system is shown in Figure 1. In this system, coal (point 1) is reacted with air (point 2) and oxygen produced in the electrolyzer (point 15) to produce hot flue gas (FG) (point 3). Hot flue gas supplies the energy needs (points 3 and 4) of the evaporator of the Rankine Cycle (RC) to produce electricity by superheat organic working fluid (points 5 and 6). It is passed through absorber of absorption chiller (points 4 and 9) to produce cooling. After removing sulfur compounds (point 10), the flue gas is reacted with hydrogen supplied by the electrolyzer (point 12) to produce syngas (CH_4) point 13. Produced syngas (point 13) is pressurized in the compressor (point 14) and it is stored in the pressure vessel for various applications. The electricity needs of compressor and electrolyzer are supplied by the electrical production of the wind turbine and Rankine cycle (steam power plant).

Extra electrical power production can be used by the user. The fuel of this system is coal and the outputs are cooling produced by absorption chiller, electrical power produced by both Rankine cycle and wind turbine, and syngas product.

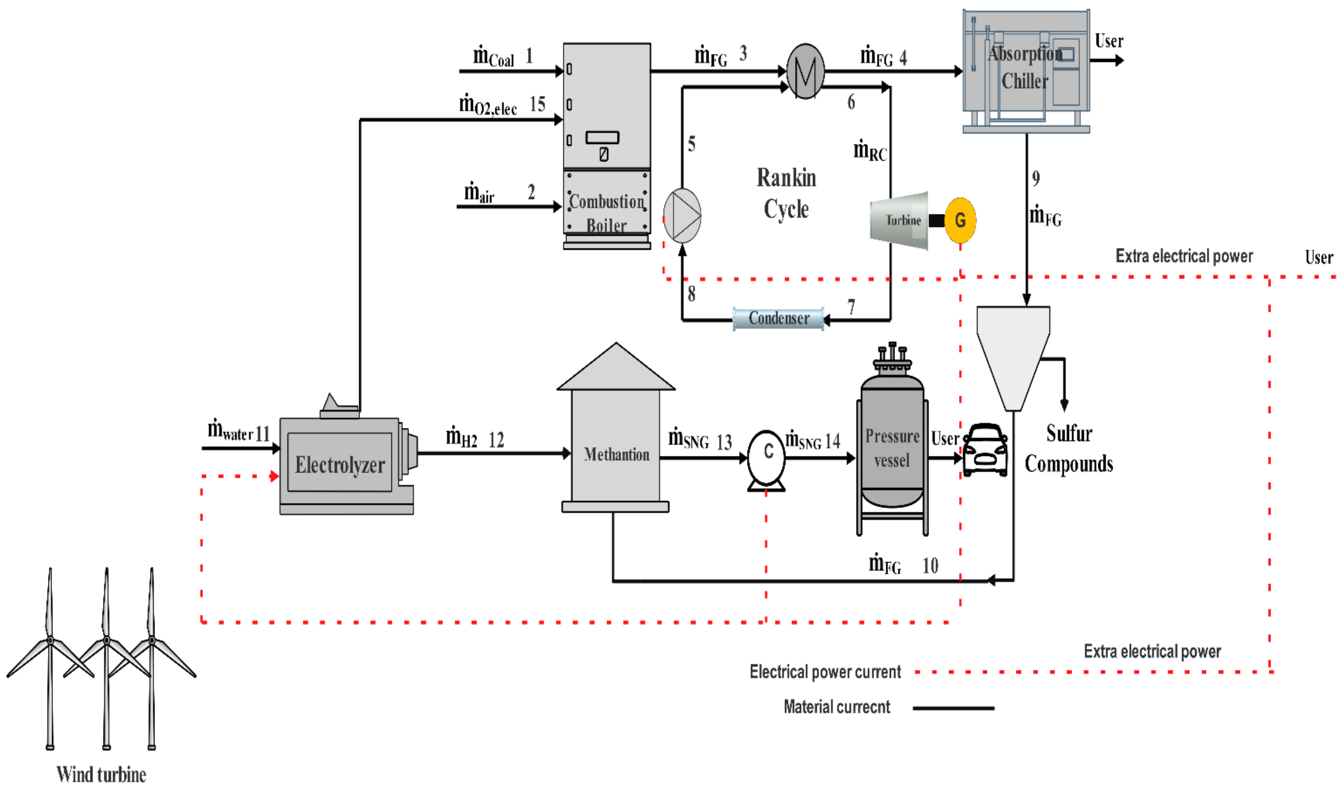

Figure1. Schematic diagram of the system

The considered assumptions in this model are as follows:

1- The system is at steady state.
2- Initial state condition is 15 °C and 1 atm.
3- Combustion boiler efficiency is 0.92.
4- The process in the pump and turbine is polytropic.

5- For the wind speed, the Weibull distribution density function is considered to calculate the power production by the wind turbine.
6- The polytropic efficiencies of the pump, turbine, and compressor are 0.85.
7- Pressure loss is assumed to be 2%.
8- Flue gas loss is assumed to be 3%.
9- Evaporator and condenser heat transfer efficiencies are assumed to be 90%.

2.2. Mass and energy balances

Based on the ultimate analysis of coal, the needs of oxygen and air mass flow rate for coal combustion are calculated by (Bailera et al., 2015):

$$\dot{m}_{O2} = \dot{m}_{Coal} r_a (2.667x_C + (8x_H - x_O) + x_S) \quad (1)$$

$$\dot{m}_{air} = 4.32\dot{m}_{Coal} r_a (2.667x_C + (8x_H - x_O) + x_S) \quad (2)$$

In equation 1, the parameter x is the weight fraction, C, H, O and S denote carbon, hydrogen, oxygen and sulfur, r_a represents air fuel ratio.

The alkaline electrolyzer is used to split water into hydrogen and oxygen. In general, the reaction presented by equation 3 takes place in the electrolyzer(Tijani et al., 2014; Ulleberg, 2003):

$$H_2O\ (l) + \text{electrical energy} \rightarrow H_2\ (g) + O_2\ (g) \quad (3)$$

The operating voltage in each cell of the electrolyzer is calculated by (Tijani et al., 2014; Ulleberg, 2003):

$$V_{cell} = V_{rev} + V_{act} + V_{ohm} \quad (4)$$

In equation 4, subscripts rev, act and ohm denote reversible, activation and ohmic. The calculation equations for $V_{rev} V_{act}$ and V_{ohm} are presented in Table 1 (Tijani et al., 2014; Ulleberg, 2003).

Table 1. Calculation equations for V_{rev}, V_{act} and V_{ohm}

No	Parameter	Equation
1	V_{rev}	$\frac{\Delta G}{2F}$
2	V_{act}	$S \log \left(\frac{\left(t_1 + \frac{t_2}{T_{elec}} + \frac{t_3}{T_{elec}}\right.}{A} I + 1\right)$
3	V_{ohm}	$\frac{(r_1 + r_2)\, T_{elec}}{A}$

In Table 1, ΔG is the Gibbs energy (237.2 $\mathrm{kJ/mol}$), F is the Faraday`s constant (96495 $\mathrm{C/mol}$), A is the area of the electrode, I is the current, r_1 and r_2 are the ohmic resistance parameters, t_1, t_2, and t_3 are the electrode overvoltage coefficients.

The current efficiency of alkaline electrolyzer can be expressed as follows (Tijani et al., 2014; Ulleberg, 2003):

$$\eta_F = \frac{\left(\frac{I}{A}\right)^2}{f_1 + \left(\frac{I}{A}\right)^2} f_2 \tag{5}$$

In equation 5, f_1 and f_2 are the parameters related to electrolyzer and Faraday efficiencies.

Hydrogen production mass flow rate in alkaline electrolyzer is calculated by (Tijani et al., 2014; Ulleberg, 2003):

$$\dot{m}_{H2} = \eta_F N_{cell} \frac{I}{F} \tag{6}$$

In equation 6, N_{cell} is the number of cells.

The power consumption in alkaline electrolyzer is calculated by (Tijani et al., 2014; Ulleberg, 2003):

$\dot{W}_{elec} = N_{cell} V_{cell}$ (7)

In the methanation plant, the reaction presented by equation 8 takes place (Bailera et al., 2015):

$CO_2 + 4H_2 \leftrightarrow CH_4 + 2H_2O$ (8)

For the wind turbine, the average electrical generated power is obtained by (Powell, 1981):

$$\dot{W}_{wind,ave} = \dot{W}_{wind,er}\left[\frac{\exp\left(-\left(\frac{u_c}{C}\right)\right)^K - \exp\left(-\left(\frac{u_r}{C}\right)\right)^K}{\left(\frac{u_r}{C}\right)^K - \left(\frac{u_c}{C}\right)^K} - \exp\left(-\left(\frac{u_f}{C}\right)\right)^K\right] \quad (9)$$

In equation 9, P_{er} is the rated power, u_c, u_r and u_f are cut-in rated and furling speeds. K, C are parameters which are calculated by (Johnson, 2006; Justus, 1978):

$$K = \left(\frac{\sigma}{\bar{u}}\right)^{-1.086} \quad (10)$$

$$C = \frac{\bar{u}}{\Gamma\left(1 + \frac{1}{k}\right)} \quad (11)$$

In equation 11, $\bar{u}$ denotes the average wind speed, Γ is the Gamma function and σ is the standard deviation.

The system component energy and mass balances, as well as energy efficiency equations, are shown in Table S1 in appendix section.

The number of wind turbines required to meet the system power consumption can be calculated by:

$$KK = \left[\frac{\dot{W}_{elec} + \dot{W}_c + \dot{W}_p - \dot{W}_T}{\dot{W}_{windturbine,ave}}\right] + 1 \quad (12)$$

The brackets ([]) mean integer function.

System energy efficiency can be calculated by:

$$\text{energy efficiency}=\frac{\dot{m}_{13}LHV_{CH_4}+KK*\dot{W}_{windturbine,ave}+\dot{Q}_{abs}+\dot{W}_T-\dot{W}_C-\dot{W}_P}{\dot{m}_1 LHV_{CH4}+KK\dot{W}_{windturbine,er}} \quad (13)$$

2.3. Exergy balance

Exergy is defined as the amount of work obtainable when some matter is brought to thermodynamic equilibrium with its surroundings. The total exergy consists of four components including kinetic exergy, potential exergy, physical exergy and chemical exergy (Bejan, 2016).

ex is the total specific exergy, calculated as (Bejan, 2016):

$$ex=(h-h_0)-T_0(s-s_0)+T_0\sum x_i\, R\, Lny_i+\sum x_i\, ex_{chi}+\frac{V^2}{2}+gz \quad (14)$$

In equation 14, h is the enthalpy, s is the specific entropy, R is the specific gas constant, ex_{chi} is the component specific chemical exergy, xi is the mass fraction, yi is the molar fraction. V is the velocity; g is the gravitational acceleration and z is the height. The notation "0" is the reference state condition (1atm, 288K).

For each component of the system, equations of exergy destruction rate and exergy efficiency are shown in Table S2 in appendix section.

System exergy efficiency can be calculated as:

$$\text{exergy efficiency}=\frac{\dot{m}_{13}ex_{ch,Ch4}+KK*\dot{W}_{windturbine,ave}+\dot{Q}_{abs}\left(1-\frac{T_0}{T_{abs}}\right)+\dot{W}_T-\dot{W}_C-\dot{W}_P}{\dot{m}_1 ex_1+\frac{8}{27}\rho A_2 U^3} \quad (15)$$

System exergy destruction is calculated by the summation of system component exergy destructions.

2.4. Economic analysis

The total investment cost represented as C_0 is obtained by the equation 16 (Bellos et al., 2019; Tzivanidis et al., 2016):

$$C_0 = K_{Wind\ turbine} + K_{Absorption\ chiller} + K_{Methanation} + K_{Elec} + K_{RC} + K_{Compressor} \quad (16)$$

In equation 16, subscripts elec defines electrolyzer component, and K denotes the investment cost of a component. The operation and maintenance costs are considered at 3% of the initial cost. For the proposed system, yearly income cash flow denoted as CF is expressed as follows (Bellos et al., 2019; Tzivanidis et al., 2016):

$$CF = Y_{electrical}k_{electrical} + Y_{cooling}k_{cooling} + Y_{CH4}k_{CH4} - Y_{CO2}k_{CO2} - Y_{Coal}k_{Coal} \quad (17)$$

In equation 17, $Y_{electrical}$, $Y_{cooling}$, Y_{CH4} are productions of electrical,cooling,and syngas for a year . Y_{CO2} is carbon dioxide consumption in methanation plant for a year. Y_{Coal} is coal consumption in a year. $k_{electrical}, k_{cooling}, k_{CH4}, k_{Coal}$ are the prices of electrical, cooling, syngas and coal, k_{CO2} is a carbon tax. For the investment, the Internal Rate of Return (IRR) is determined by (Bellos et al., 2019; Tzivanidis et al., 2016):

$$IRR = \frac{CF}{C_0}\left[1 - \frac{1}{(1 + IRR)^N}\right] \quad (18)$$

Net Present Value (NPV) represents the total investment gain during the life time of the project that can be expressed as (Bellos et al., 2019; Tzivanidis et al., 2016):

$$NPV = -C_0 + CF\frac{(1 + r)^N - 1}{r(1 + r)^N} \quad (19)$$

In equation 19, r and N denote discount factor and project lifetime that are considered to be 3% and 25 y. The Simple Payback Period (SPP) is calculated as follows (Bellos et al., 2019; Tzivanidis et al., 2016):

$$SPP = \frac{C_0}{CF} \quad (20)$$

The Payback Period (PP) equation is as follows (Bellos et al., 2019; Tzivanidis et al., 2016):

$$PP = \frac{\ln(\frac{C_F}{CF - r.C_0})}{\ln(1 + r)} \quad (21)$$

Each index is independent of another one, which makes them significant individually. The initial cost functions and values are presented in Table S3 in appendix section.

3. Results and discussion

For mathematical modeling, a computational program was written in MATLAB software. This program is divided into one main program and two functions for calculating the fluid properties and wind turbine power production.

3.1. System specification

The ultimate analysis of coal is shown in Table 2 (Verma et al., 2010).

Table 2. Ultimate analysis of coal (weight based)

x_C	x_H	x_O	x_N	x_S	x_M	x_Z
65.72	5.27	7.1	1.29	1.69	8.09	10.84

The type of wind turbine is Nordic wind turbine with 1000 kW rated power. Specification of this wind turbine is shown in Table 3.

Table 3. Nordic wind turbine specification

No	Parameter	Unit	Value
1	$\dot{W}_{windturbine,er}$	kW	1000
2	u_C	m/s	4
3	u_r	m/s	16

4	u_f	m/s	22
5	h	m	70
6	A	m^2	2732

The system specification is shown in Table 4. The wind velocity value at a certain speed for Tehran is shown in Table S4 in the appendix section (Atabi et al., 2014).

Table 4. System specification

No	Parameter	Unit	Value
1	$\dot{m}_1$	kg/s	0.04
2	r_a	Molar basis	2.34
3	LHV_{coal}	kJ/kg	27213
4	T_{elec}	K	353.15
5	T_1	K	288.15
6	T_2	K	288.15
7	T_4	K	368.15
8	T_6	K	1324.1
8	T_9	K	338.15
9	P_5	kPa	8104
10	P_6	kPa	8104
11	P_7	kPa	40.5
11	P_8	kPa	40.5
11	T_{pinch}	oC	30

12	η_{CC}	-	0.92
13	η_{C}	-	0.9
14	η_{E}	-	0.9
15	η_{T}	-	0.85
16	η_{P}	-	0.85
17	η_{Com}	-	0.85
18	COP	-	0.87
19	r_{C}	-	8
20	$\dot{m}_{RC}$	kg/s	0.1817

In Tables 3 & 4, r_a is the air-fuel ratio (mass basis), T_{pinch} is the temperature difference between hot gas and superheated steam, η_{CC} represents the combustion chamber efficiency. η_T, η_P, and η_C are turbine, pump and compressor polytrophic efficiencies, COP defines the absorption chiller coefficient of performance, r_c is the compression factor of compressor, $\dot{W}_{windturbine,er}$ is the rated power of wind turbine, u_c, u_r and u_f are cut-in, rated and furling speeds of the wind turbine, h is the tower height of the wind turbine and A is the swept area wind turbine.

Figure 2 shows the monthly average wind turbine electrical power production during one year.

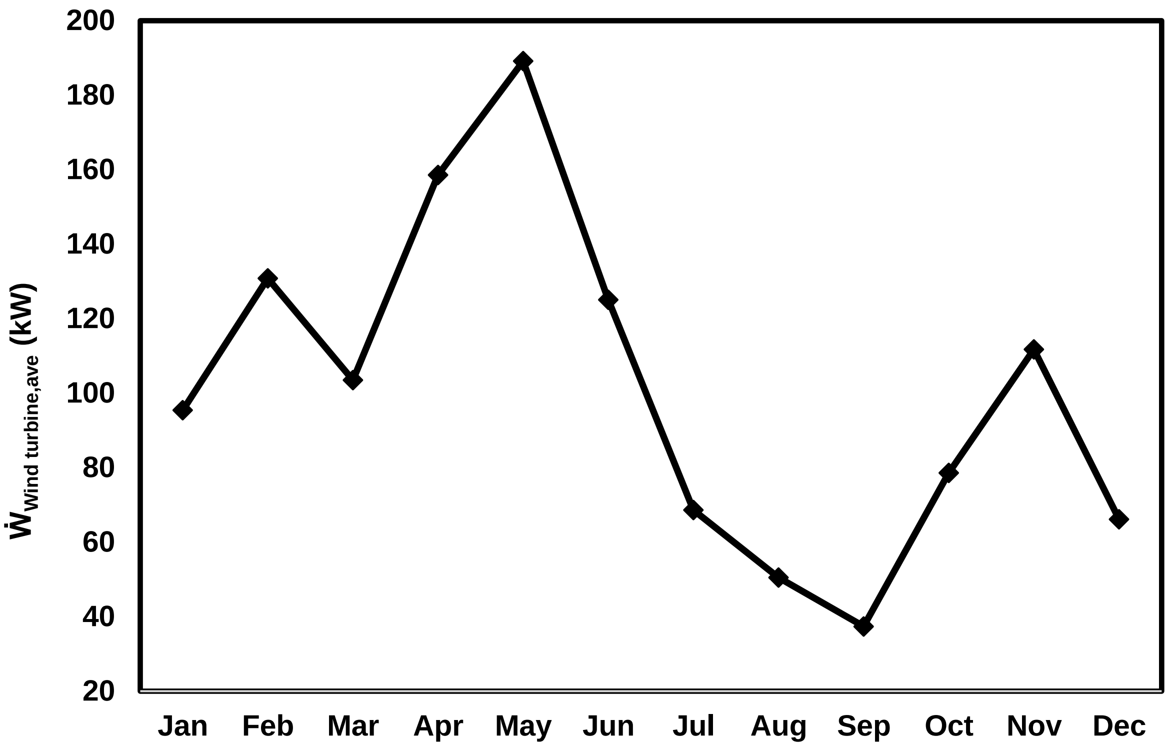

Figure 2. Monthly average wind turbine electrical power production during various months of a year

Table 5 shows the main system parameters calculated by the program.

Table 5. Results of the main parameters

No.	Parameter	Unit	Value
1	$\dot{W}_{elec}$	kW	3214.2
2	$\dot{W}_{P}$	kW	1.65
3	$\dot{W}_{T}$	kW	243.4
4	$\dot{W}_{C}$	kW	16.2
5	$\dot{Q}_{abs}$	kW	22.6

Based on equation 12, Table 3, and Figure 2, the required number of Nordic wind turbine units is shown in Figure 3. According to Figure 3, the maximum number of wind turbines needed in September is equal to 80. Since the conversion of all the carbon dioxide in flue gas is guaranteed by this system, the total number of 80 of 1 MW Nordic wind turbine units is selected. For the other months of a year, the extra electrical power production can be delivered to electrical network.

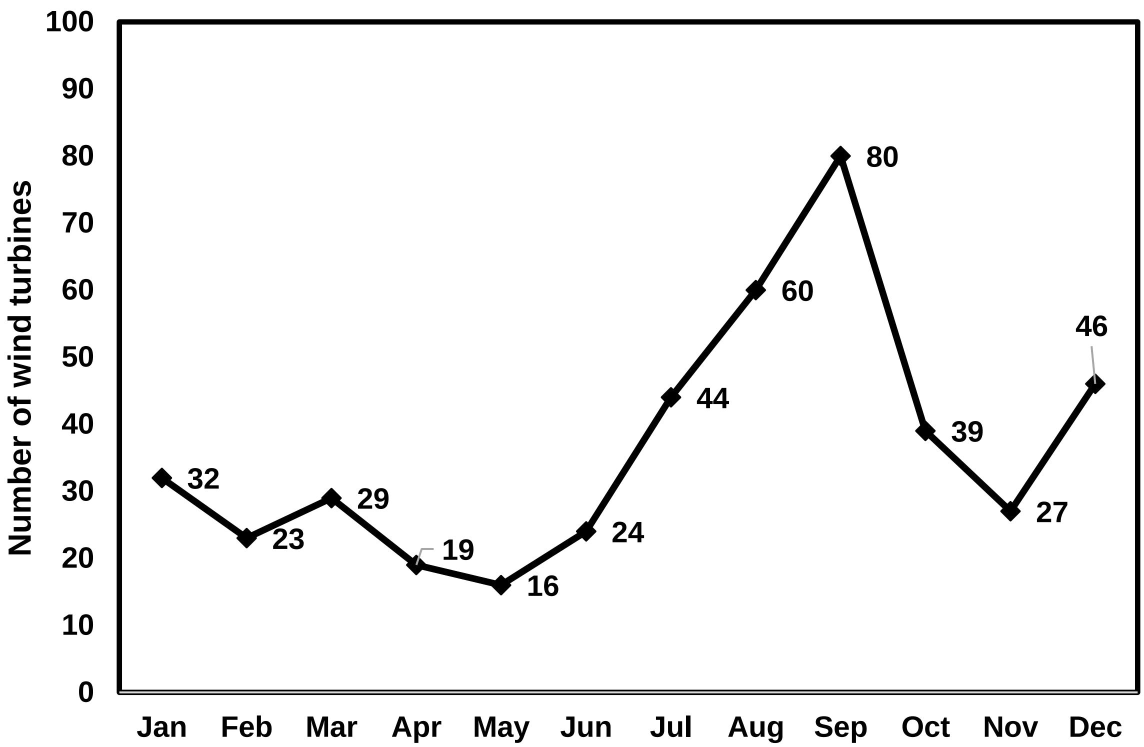

Figure 3. Required number of the Nordic wind turbine units

Table 6 shows the system comparison with and without syngas production during a year. Power for syngas production system is required in electrolyzer, compressor, and methanation plant. The consumption of electrical power to produce syngas is calculated to be equal to 25.6 MWh/t.

Table 6. System comparison with and without syngas production

No.	Parameter	Unit	Value	
			With syngas	Without syngas
1	$\dot{m}_{CO2}$ consumption	t/y	2776	0
2	$\dot{m}_{H2}$ consumption	t/y	504.7	0

3	$\dot{m}_{Coal}$ consumption	t/y	1152	1152
4	$\dot{m}_{syngas}$ production	t/y	1009.4	0
5	$\dot{Q}_{abs}$ cooling production	MWh	180.5	180.5
6	electrical power production	MWh	40920.4	66763.1

3.2. Validation of theoretical model

Since a similar complex system has not been investigated yet, the validation of the whole system is impossible. Each of the main components is validated individually. The average power production of the Nordic wind turbine is compared with the manufacturer power curve shown in Ref. (Pierrot, 2019).

Regarding wind velocity information of Tehran (province of Iran) shown in Table S4, the annual average power produced by the Nordic model wind turbine is calculated to be 103.1 kW by equation 9 while it is 94.3 kW by power curve. The error is around 8%, which can be due to the following reasons:

1) Equation 9 uses the statistical data of the wind turbine while the power curve is based on production power versus wind velocity.

2) The height of the tower is not determined in Ref. (Pierrot, 2019) and it is between 60 to 70 m, which has an effect on the power produced by the wind turbine.

3) For the power curve, the air density is considered to be 1.225 kg/m^3, while this value may differ for Tehran

For the alkaline electrolyzer, the theoretical model used in this study was validated before (Ulleberg, 2003). Figures 6 to 10 of this reference were compared to the simulation and experimental data. For example, in Figure 7 of this reference, the root means square (RMS) error for hydrogen production is 0.053 Nm^3/hr (in the range of 1 to 3 Nm^3/hr hydrogen production).

For validation of the combustion chamber, the exhaust gas temperature was compared with Ref. (Anderson). In this reference, the process flow diagram (PFD) of one real coal-fired steam power plant is given. The hot exhaust gas temperature is determined to be $1259.2\ ^0$C. By inserting the fuel and air ratios to computational code, this temperature is calculated to be $1324.6\ ^0$C. The error is about 4.9%. The main reasons for this error are as follows:

1) The coal composition is not specified and may be different
2) The distribution of the coal and air is different in the combustion chamber and the combustion is not uniform in real conditions

The plant energy efficiency in that reference is about 35.2%, while it is about 30.1% in this study and the mean error is about 14% because of the lack of information about the main parameters in that reference. The steam turbine used in that reference has three stages (i.e., high, medium and low pressure steam), while the one stage steam turbine is considered in this study. The pure oxygen produced by the electrolyzer is injected to the burner, which brings another different feature between the two systems. The steam power plant energy efficiency is in a reasonable range. For further evaluation, the Ref (Suresh et al., 2012) is considered. The main configuration is modeled in the code. The plant energy efficiency is calculated at around 29.1%, which is consistent with the plant energy efficiency shown in that ref (29.3%).

3.3. System energy and exergy analyses

Figure 4 shows the annual average energy efficiency of various components of the system. The highest and lowest energy efficiencies are related to the compressor and steam power plant.

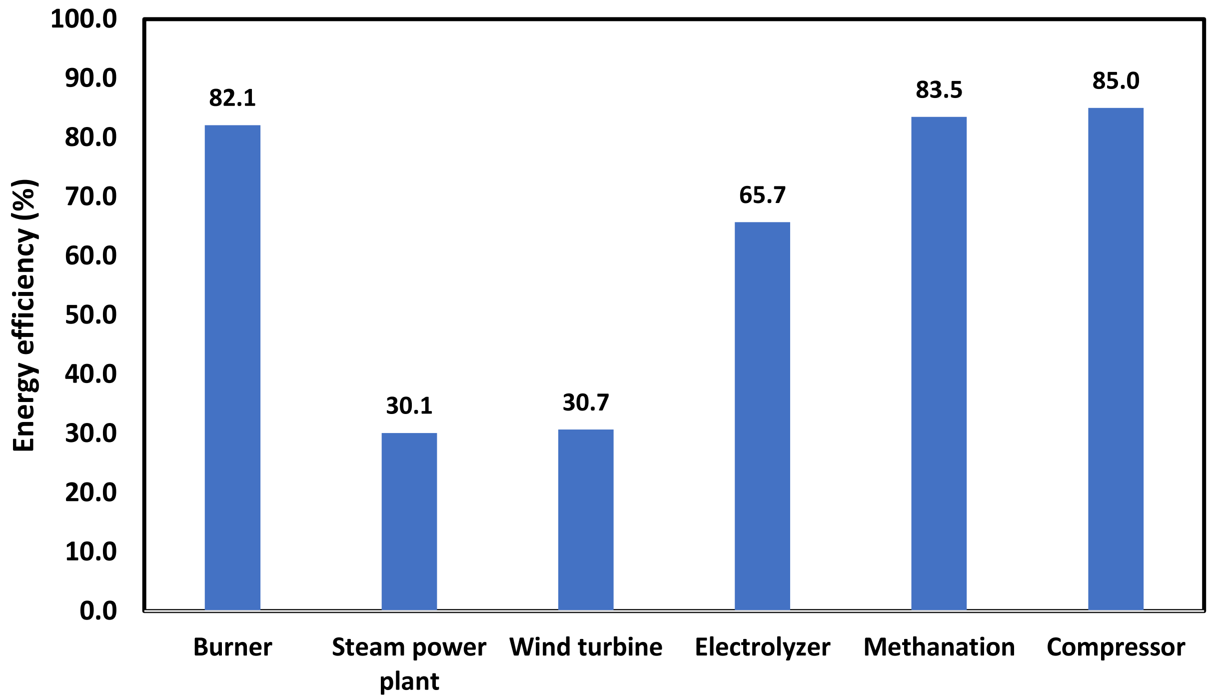

Figure 4. Annual average energy efficiencies of various system components.

Figure 5 shows the annual average exergy efficiency of various components of the system. Compared with Figure 4, although the highest exergy efficiency is still related to the compressor, the lowest exergy efficiency is here related to the wind turbine.

Exergy efficiency of the burner is lower than its energy efficiency. From the exergy viewpoint, this phenomenon is due to the fact that chemical reactions usually reduce exergy efficiency and increase the exergy destruction rate. This phenomenon is also true for the electrolyzer and the methanation plant. Wind turbine exergy efficiency is usually lower than wind turbine energy efficiency. The difference between energy and exergy efficiencies is because power rate of wind turbine is considered for thermal efficiency. For exergy efficiency, the exergy of wind velocity is considered (numerator of wind turbine exergy efficiency).

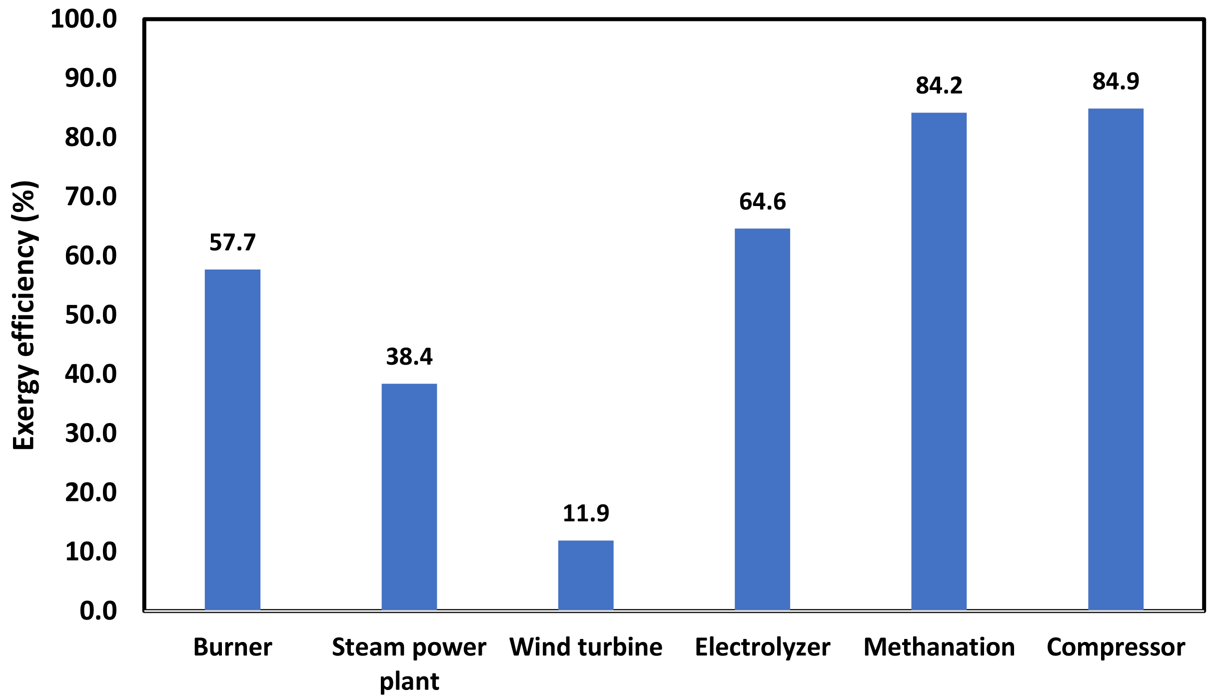

Figure 5. Annual exergy efficiency of various system components

Figure 6 represents the annual average exergy destruction rate for each component of the steam power plant (Rankine cycle). The maximum exergy destruction rate is related to the evaporator because of the heat absorbed from the hot flue gas (points 3 and 4). Heat transfer is generally one of the main sources of exergy destruction. Power consumption of pumps is usually very low in the steam power plants; the exergy destruction is also low as a result. In the condenser, since heat is dissipated to the environment, exergy destruction is very low.

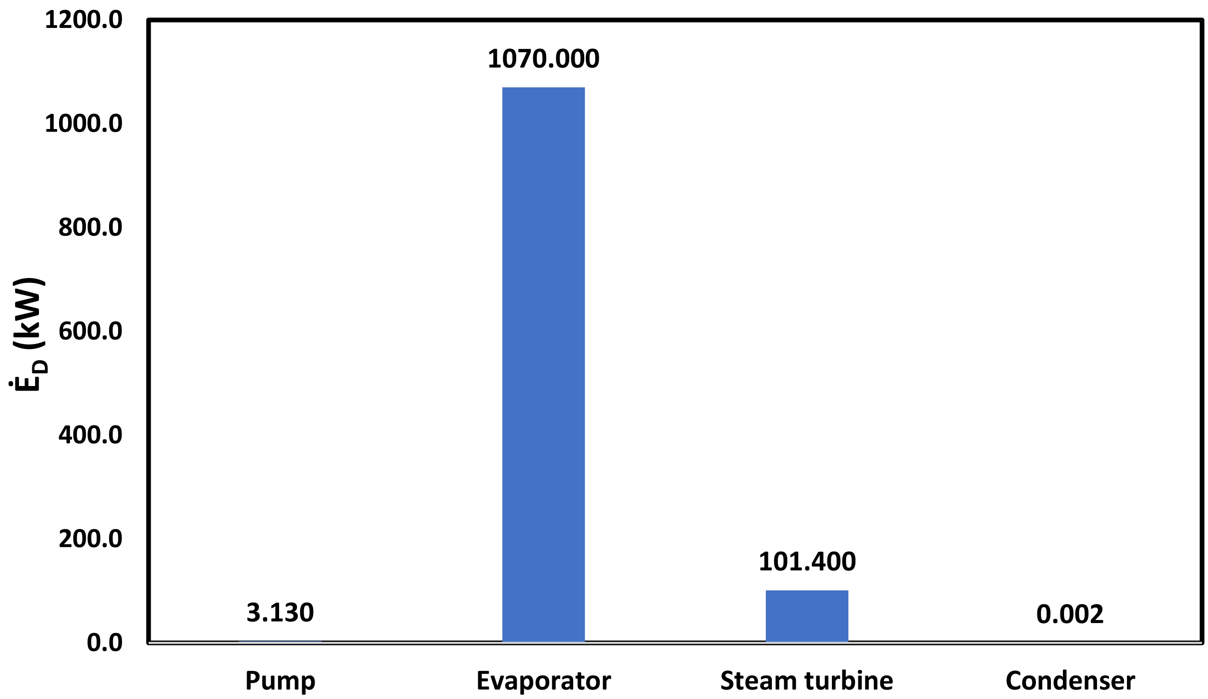

Figure 6. Annual average exergy destruction rate for various components of steam power plant

Figure 7 shows the annual average exergy destruction rate for various components of the system. The maximum exergy destruction rate is related to the steam power plant which is equal to 1174.5 kW. Since the steam cycle includes four components (evaporator, pump, steam turbine, and condenser) and all of them have significant exergy destruction rates, their summation is considerable.

The exergy destruction rate in electrolyzer is also high (1086.4 kW) due to chemical reaction. Exergy destruction in methanation and burner are considerable due to the same reason of electrolyzer.

The exergy destruction in one wind turbine is equal to 501.2 kW. It can be concluded that the main part of wind velocity exergy is wasted in the wind turbine.

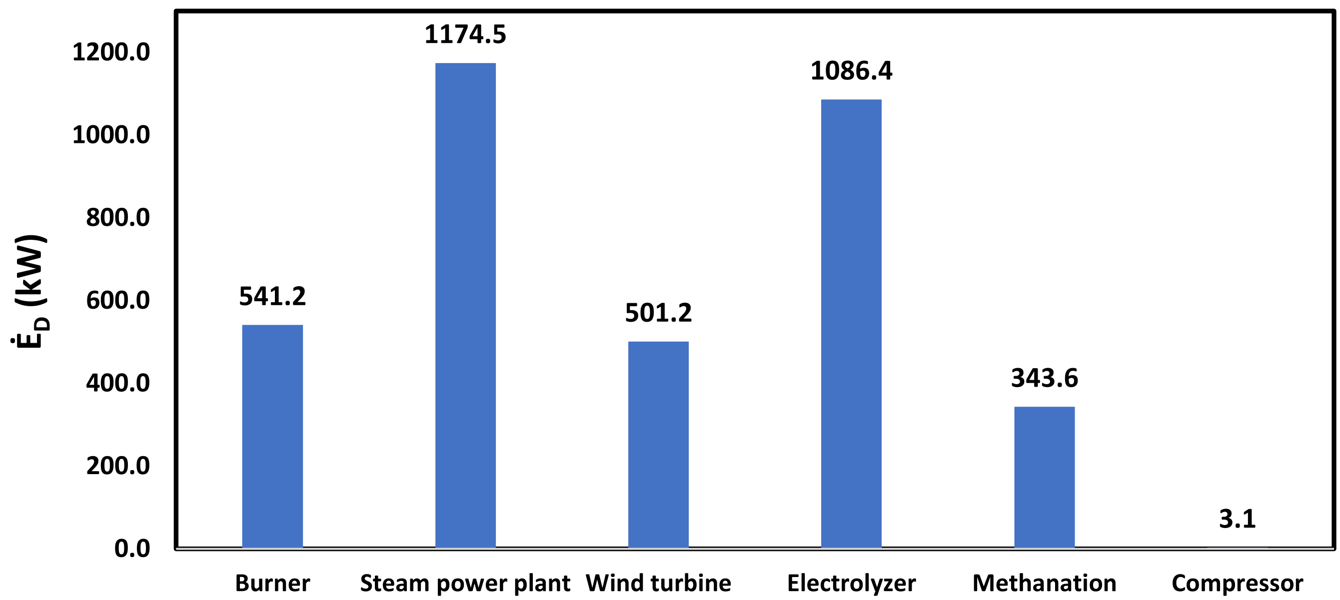

Figure 7. Annual average exergy destruction rate for various components of the system

Figure 8 illustrates the system energy and exergy efficiencies. Energy efficiency is slightly higher than exergy efficiency. In comparison to Figure 4, it is clear that system thermal efficiency is lower than all of the energy efficiencies of system components. In comparison to Figure 5, exergy efficiency of the system is higher than wind turbine exergy efficiency and lower than exergy efficiency of other system components.

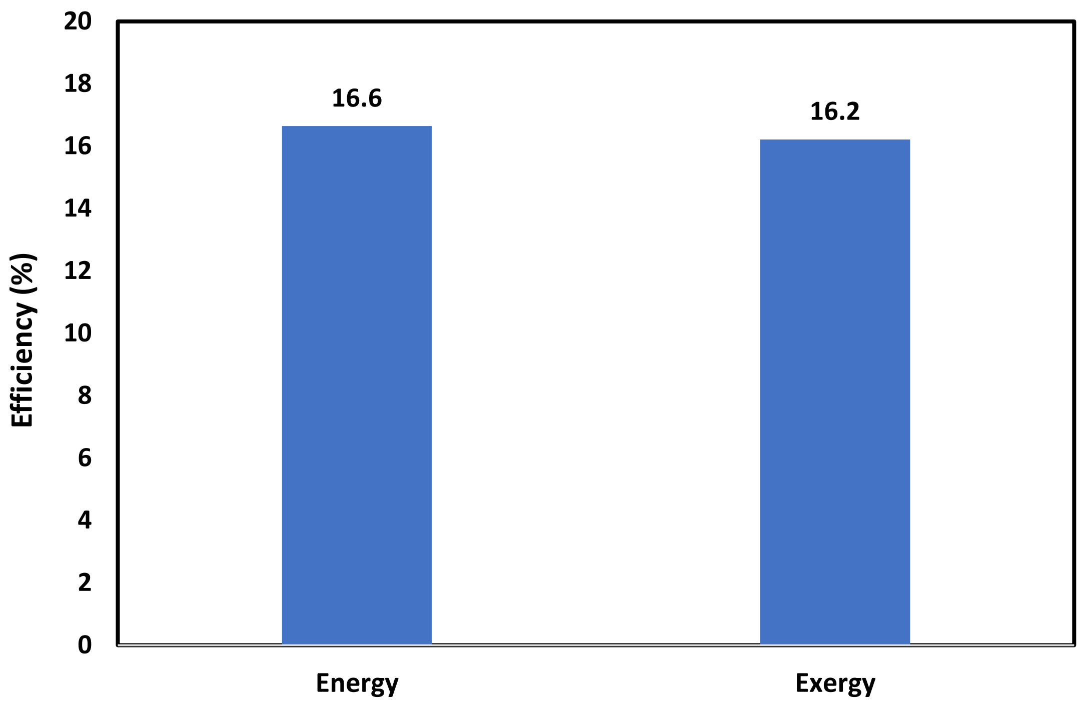

Figure 8. System energy and exergy efficiencies

3.4. System economic analysis

Regarding the system economic analysis, the costs of coal as well as electricity, cooling, syngas and carbon tax are considered according to Table 7.

Table 7. Cost of products and consumption of the system

No.	Products and consumptions of system	Unit	Cost	References
1	$k_{electrical}$	$/kWh	0.22	(Bellos et al., 2019; Bellos et al., 2016; Bellos et al., 2017; Kreuter and Hofmann, 1998; Nakomčić-smaragdakis and Dragutinović, 2016; Tzivanidis et al., 2016)
2	$k_{cooling}$	$/kWh	0.074	(Bellos et al., 2019; Bellos et al., 2016; Bellos et al., 2017; Kreuter and Hofmann, 1998; Nakomčić-smaragdakis and Dragutinović, 2016; Tzivanidis et al., 2016)
3	k_{CH4}	$/kWh	0.12	(Bellos et al., 2019; Bellos et al., 2016; Bellos et al., 2017; Kreuter and Hofmann, 1998; Nakomčić-smaragdakis and Dragutinović, 2016; Tzivanidis et al., 2016)
4	k_{Coal}	$/t	66.58	(Guandalini et al., 2017)
5	k_{CO2}	$/t	31.2	(Bellos et al., 2019; Bellos et al., 2016; Bellos et al., 2017; Kreuter and Hofmann, 1998; Nakomčić-smaragdakis and Dragutinović, 2016; Tzivanidis et al., 2016)

Table 8 shows the economic investigation results for the system with and without syngas production system. Syngas production system is including electrolyzer, methanation and compressor. The PP for the system with or without syngas production are calculated to be 11.2 and 7.4 y, and this difference could be justified by considering the components required for syngas production. The NVP for the system with or without syngas production is respectively 1.6 and 8.45 US$. The IRR index for the system with or without syngas production is 10 and 15 %.

Table 8. Economic investigation results for the system with and without syngas production

No.	Parameter	Unit	Values	
			With syngas	Without syngas
1	SPP	y	9.4	6.6
2	PP	y	11.2	7.4
3	IRR	%	0.1	0.15
4	NPV	US$	1.6×10^8	8.45×10^7
5	C0	US$	1.03×10^8	9.83×10^7
6	CF	US$	1.09×10^7	1.49×10^7

3.5. System sensitivity analysis

Figure 9 presents the relation between coal mass flow rate consumed by the system and syngas production. This relation is semi-linear. By changing the coal mass flow rate in the range of 0.01 to 0.1 kg/s, the syngas production mass flow rate is increased from 0.009 to 0.088 kg/s. This is because CO_2 production increases linearly with mass flow rate of coal and syngas production shows the same trend as CO_2 production.

Figure 10 shows the evolution of electrical consumption of alkaline electrolyzer as a function of coal mass flow rate burned in the burner. Similar to Figure 9, the relation is semi-linear. This is because hydrogen need increases linearly with CO_2 production as well as coal consumption. The power consumption of electrolyzer exhibits a semi-linear relationship with hydrogen production in this system.

It can be concluded that the electrical consumption of alkaline electrolyzer represents the highest portion of system electrical consumption.

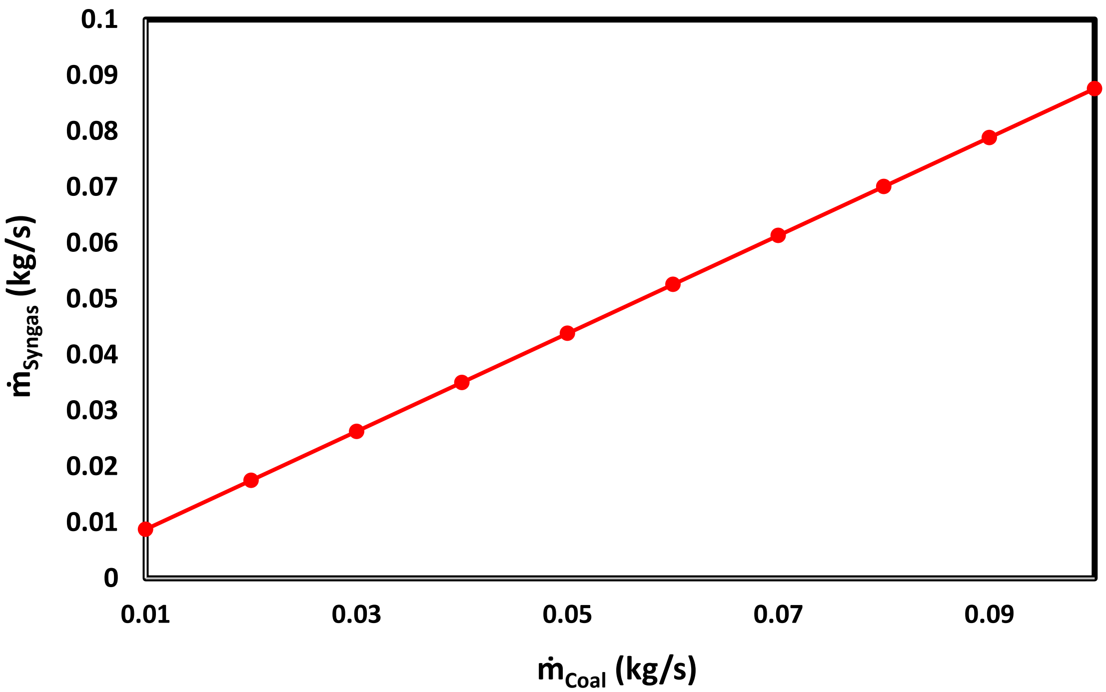

Figure 9. System syngas production versus coal mass flow rate consumption

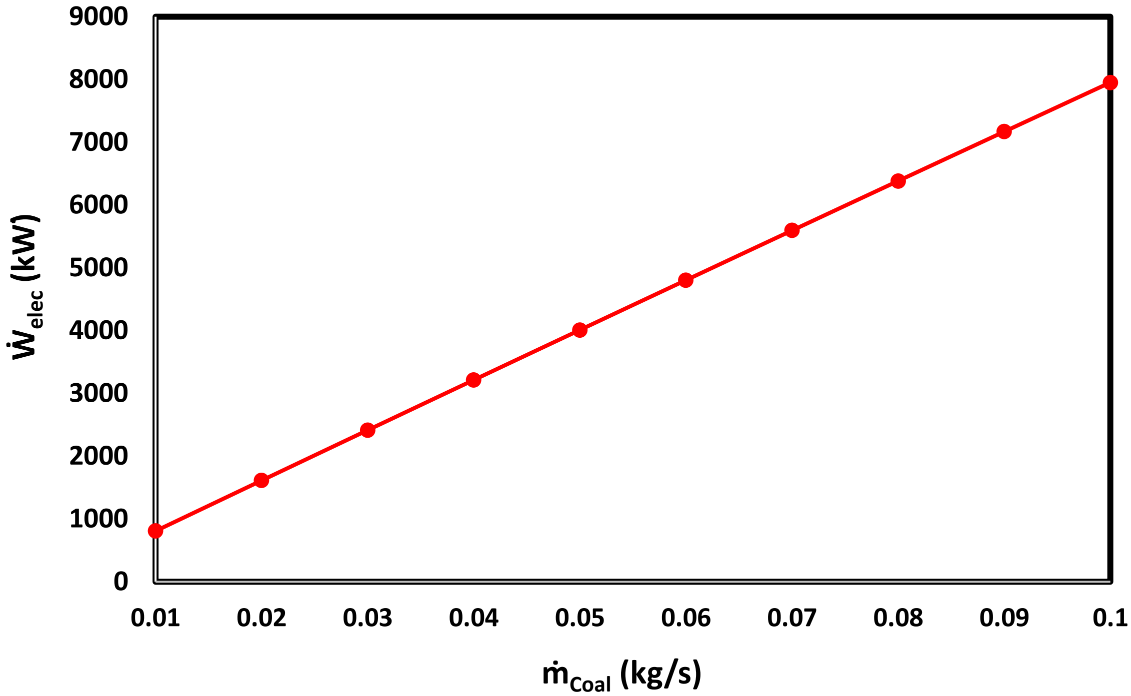

Figure 10. Evolution of electrical consumption of alkaline electrolyzer with coal mass flow rate

The effect of coal mass flow rate on variation of cooling produced in absorption chiller is reported in Figure 11. By increasing the coal mass flow rate in the range of 0.01 to o.1 kg/s , the cooling produced in the absorption chiller is varied from 5.6 to 56.4 kW. Increasing the coal mass flow rate generates additional exhaust gas from the combustion chamber, thereby increasing the energy content of exhaust gas, which in turn enhances (linear dependency) the cooling produced in the absorption chiller (according to equation of absorption chiller shown in Table S1).

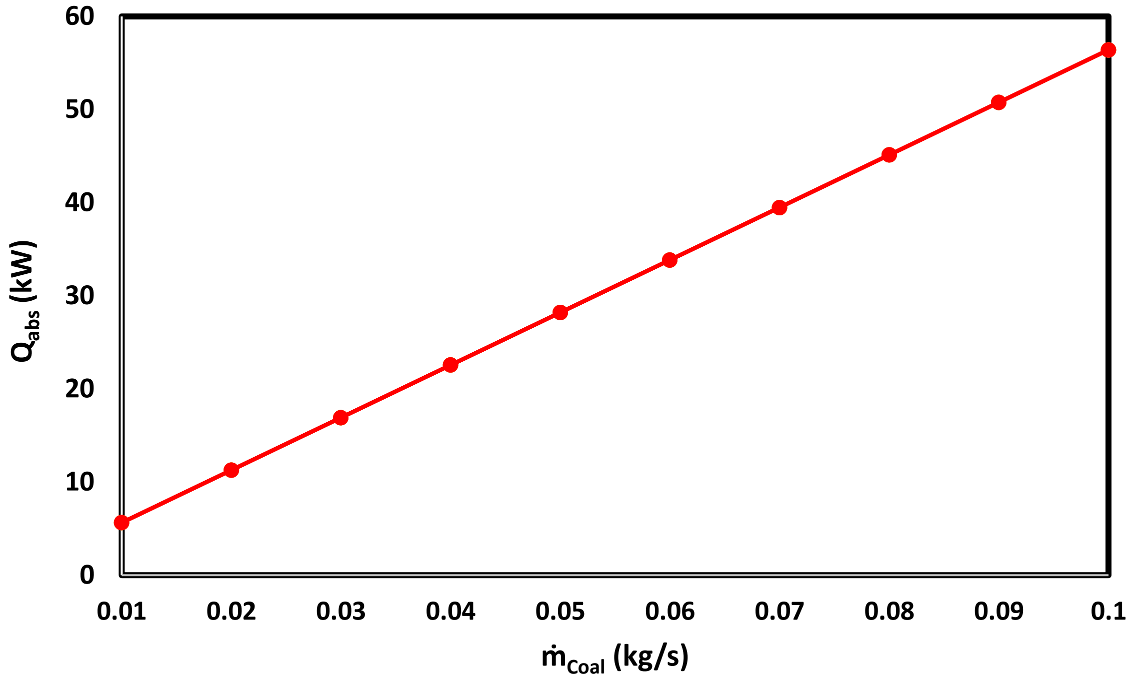

Figure 11. Variation of absorption chiller cooling production with coal mass flow rate

Figure 12 shows the system energy efficiency variation with the coal mass flow rate. The maximum system energy efficiency is reached for coal mass flow rate of 0.1 kg/s. The effect of coal mass flow rate on system energy efficiency is not considerable.

The following impacts on the system can be observed by increasing the coal mass flow rate:

1) According to the equation 12, by increasing the coal mass flow rate the number of wind turbines is increased to meet the electrical energy needs of electrolyzer. According to equation 13, this increase has an effect on system energy efficiency (wind turbine power production and rated power.). The system energy efficiency is decreased as a result (negative effect) due to low potential of wind in Tehran.
2) The increase of the coal mass flow rate results in the increase of the electrical power production in steam power plant and cooling production in the absorption chiller as well as syngas production

in methanation plant. According to equation 13, these phenomena lead to the increase of system energy efficiency (positive effect).

3) The increase of the coal mass flow rate causes the increase of electrolyzer power consumption (negative effect), since more oxygen should be produced to burn the coal in the combustion chamber.

From the whole contribution of these effects, the optimum coal mass flow rate is identified at 0.1 kg/s. Figure 13 shows the system exergy efficiency variation with changes in the coal mass flow rate. Similar to Figure 12, the trend of the curve is wavy due to the same reason as for the system energy efficiency behavior.

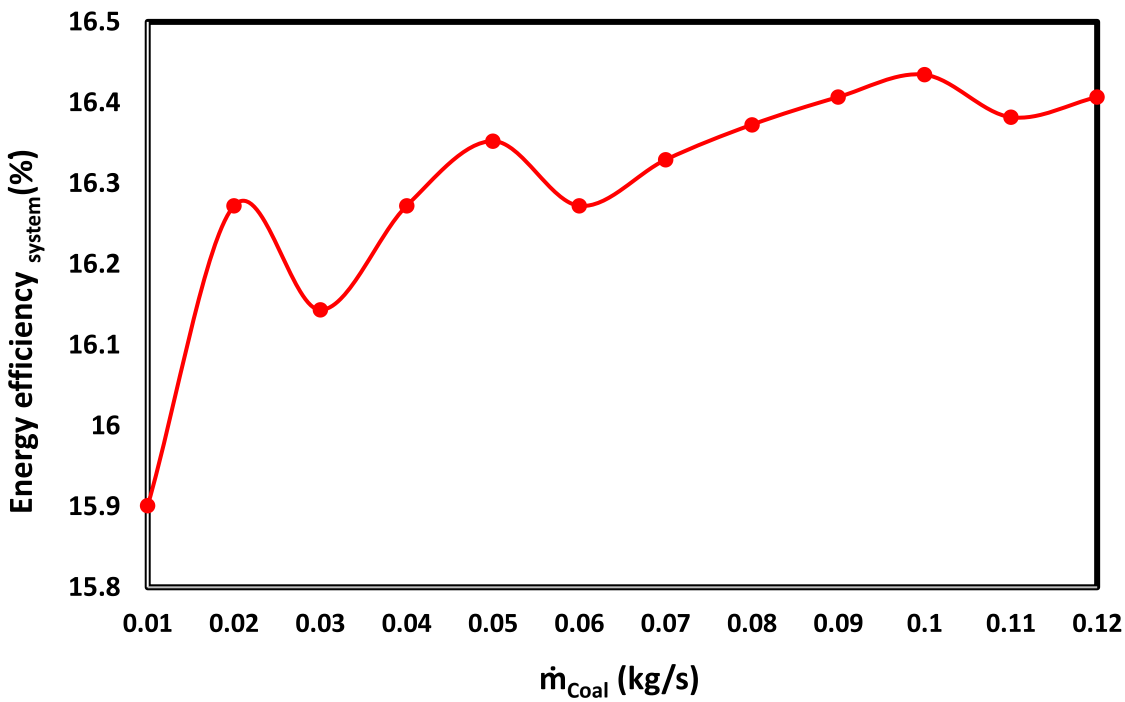

Figure 12. System energy efficiency variation with coal mass flow rate

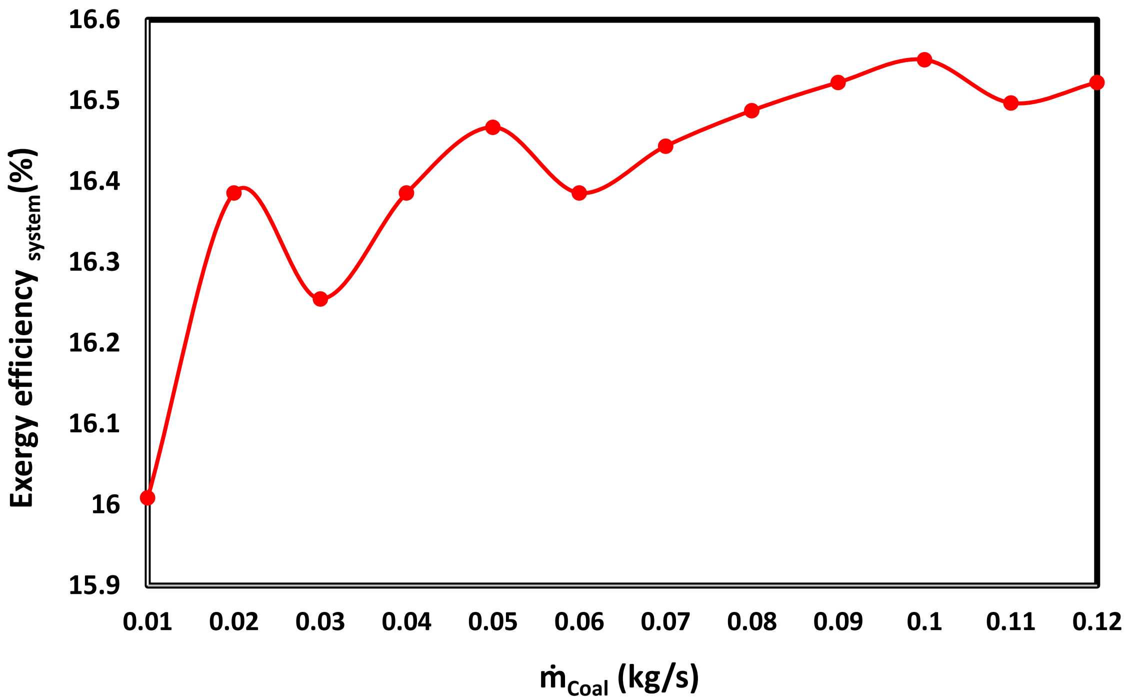

Figure 13. System exergy efficiency variation with coal mass flow rate.

The changes of system exergy destruction rate with variation of coal mass flow rate are presented in Figure 14. In contrast to the system energy and exergy efficiency evolutions, the trend of this curve is linear. This phenomenon is due to the fact that increasing the number of wind turbines only increases the exergy destruction rate. In contrast, for the system energy and exergy efficiencies, increasing the number of wind turbines has an impact on both denominator and numerator of equations 13 and 15.

Figure 15 reveals the effect of air fuel ratio on burner energy and exergy efficiencies. By increasing air fuel ratio, both the energy and exergy efficiencies of the burner are reduced. By increasing air fuel ratio, the exhaust gas temperature is decreased. Regarding equations in Tables S1 & S2, energy and exergy efficiencies are reduced. Increasing the exhaust mass flow rate also causes an increase of the number of wind turbines. This increase has a direct effect on the energy and exergy efficiencies of the system so that the trend of this curve is semi linear.

Figure 16 shows the exergy destruction rate of the burner with variation of air fuel ratio. As expected, by increasing air fuel ratio, air mass flow rate increases. The differences between inlet and outlet exergy flow rates is increased too. Since the exergy destruction is calculated based on the subtraction of inlet and outlet exergy rates, the trend of this curve is semi linear.

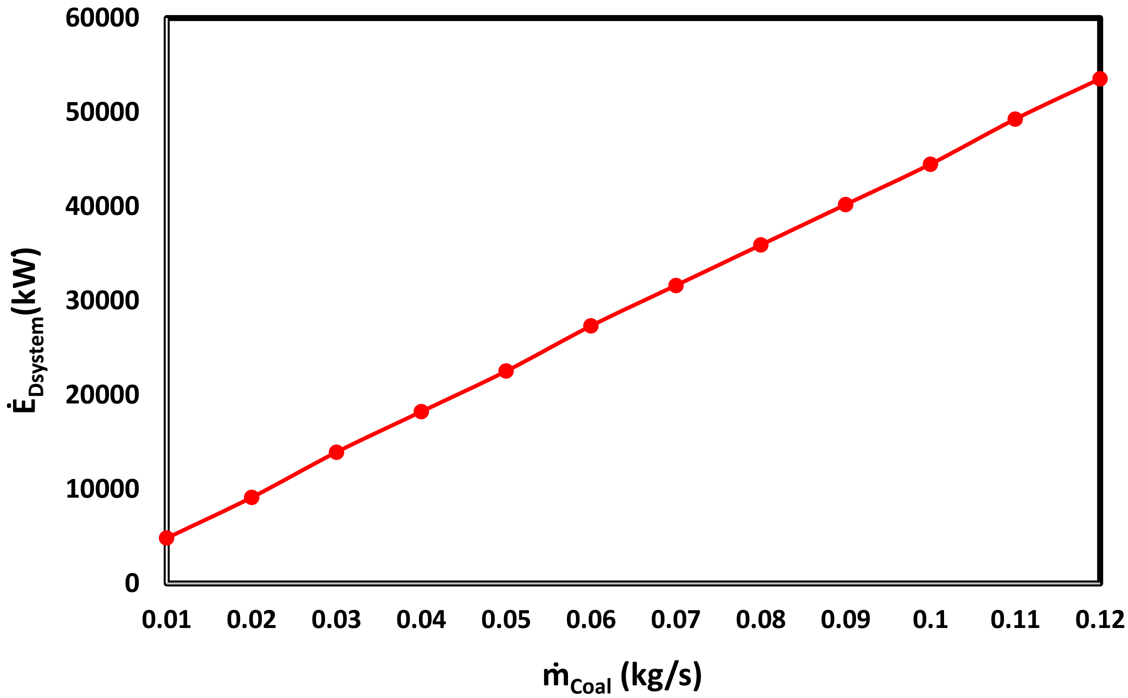

Figure 14. Effect of coal mass flow rate on system exergy destruction rate

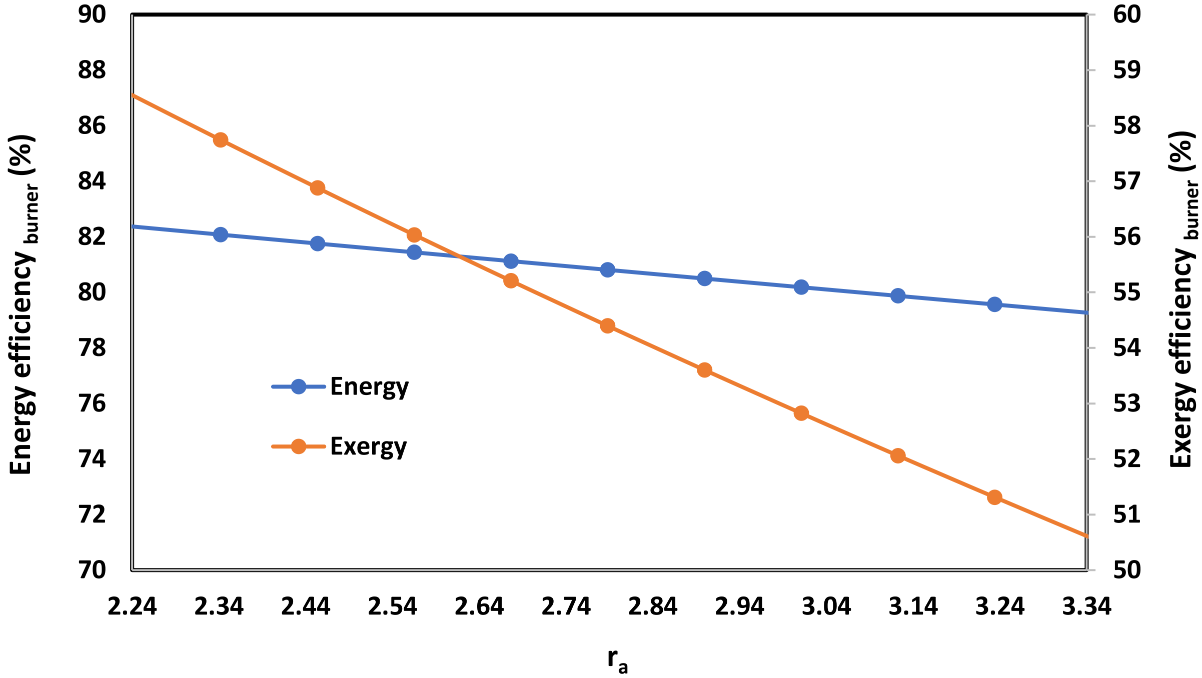

Figure 15. Effect of air fuel ratio on burner energy and exergy efficiencies

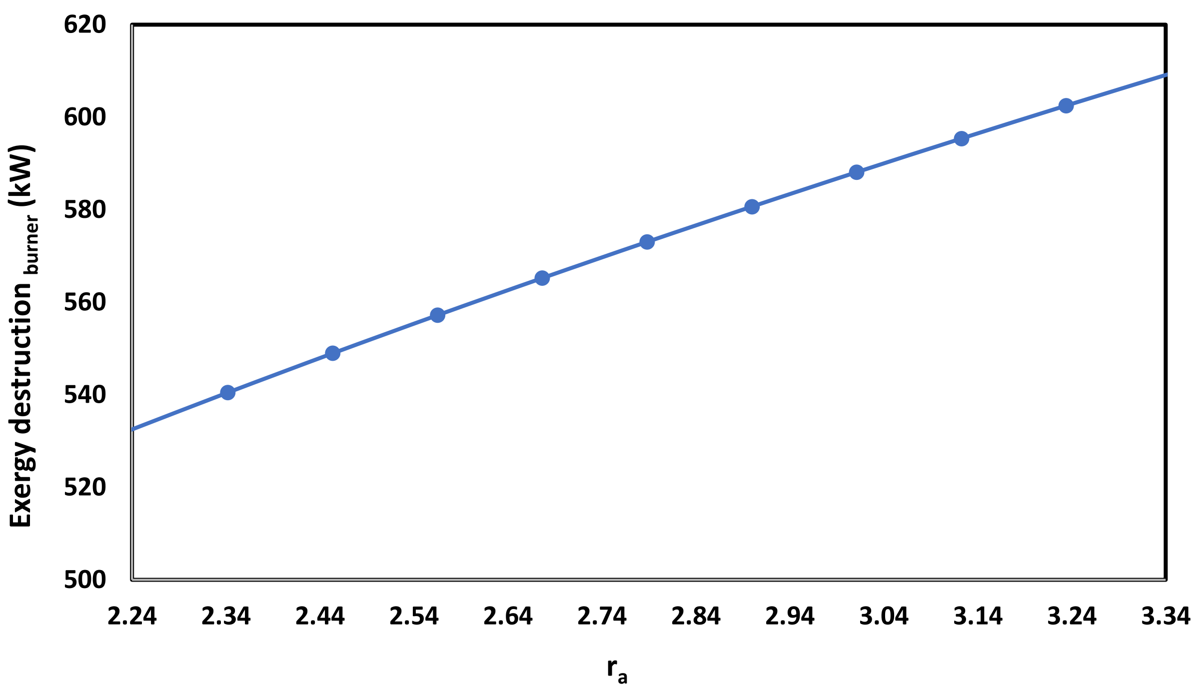

Figure 16. Effect of air fuel ratio on exergy destruction rate of the burner

The impact of air fuel ratio on the steam power plant (Rankine cycle) energy and exergy efficiencies is shown in Figure 17. When increasing air fuel ratio, the temperature of hot exhaust gas is decreased, the heat source temperature of the steam power plant is decreased. This decrease causes a reduction in energy and exergy efficiencies of the steam power plant.

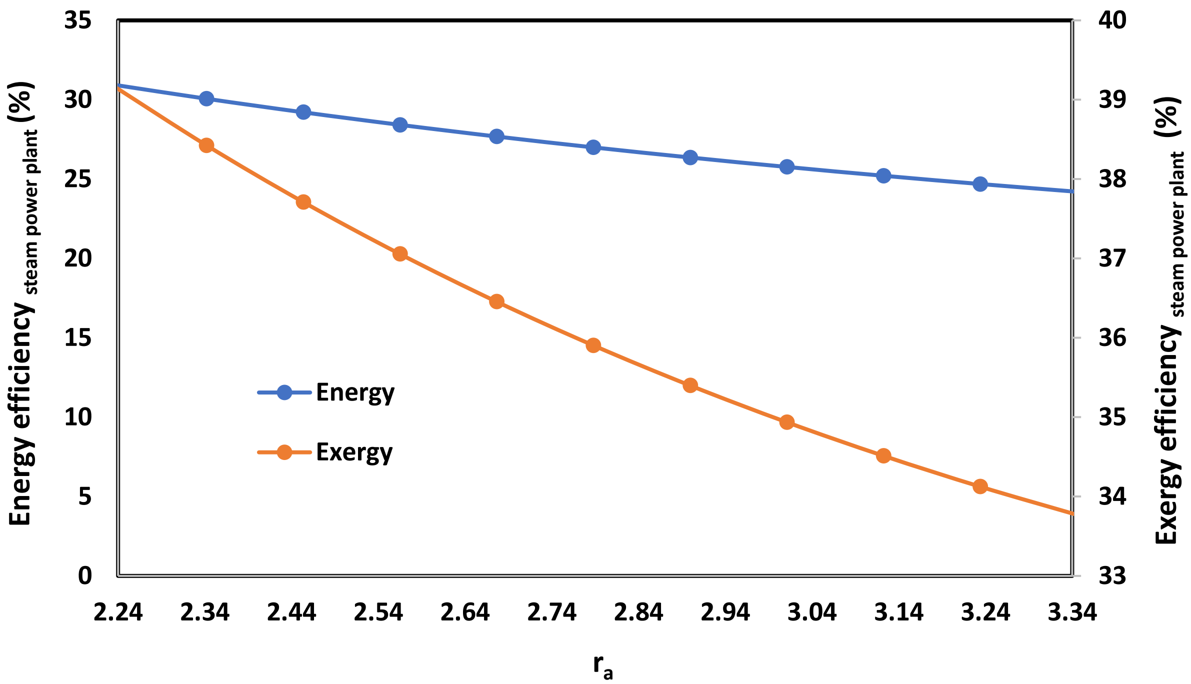

Figure 17. Variation of steam power plant (Rankine cycle) energy and exergy efficiencies with air fuel ratio

The variation of the steam power plant exergy destruction rate with changes in air fuel ratio is illustrated in Figure 18. By increasing air fuel ratio, the exhaust gas temperature is decreased. The power produced in the steam power plant as well as exergy destruction rate is decreased too.

Figure 19 reports the effect of air fuel ratio on absorption chiller exergy destruction rate. By increasing air fuel ratio, two opposing effects can be observed:

1) Decreasing gas temperature in points 3 and 4

2) Increasing mass flow rates in points 3 and 4

Although item 1 decreases the exergy destruction rate in the absorption chiller, item 2 increases this value. The item 2 overcomes item 1 so that the exergy destruction rate in absorption chiller is increased.

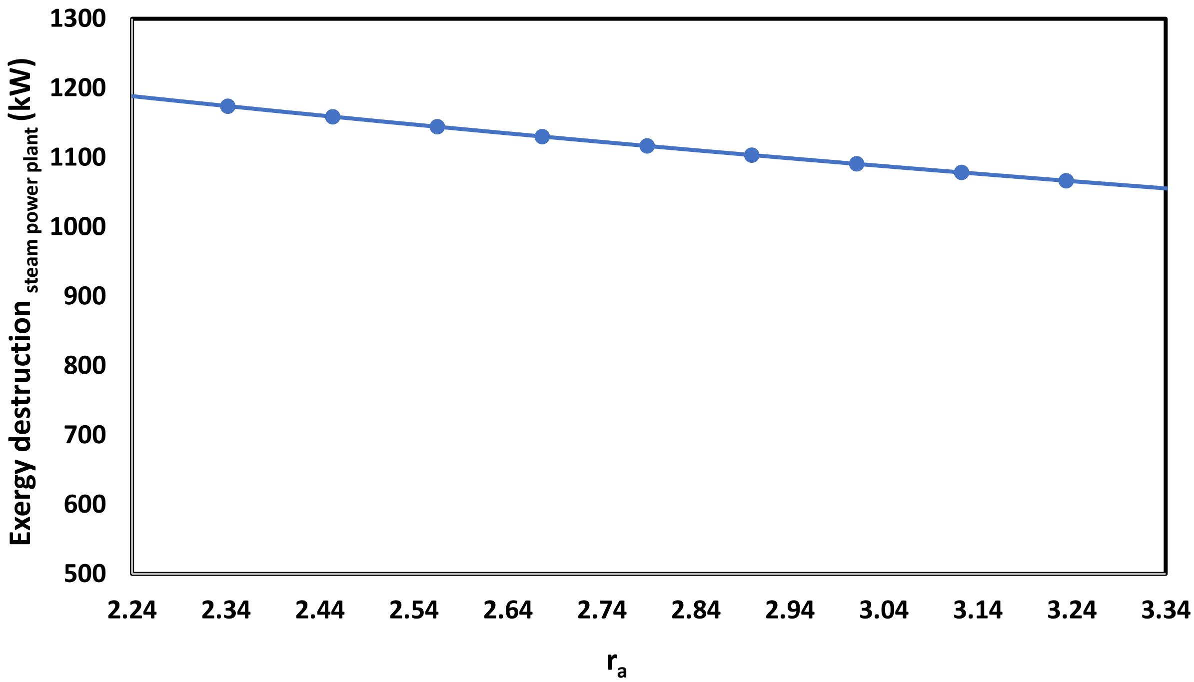

Figure 18. Variation of steam power plant exergy destruction rate with air fuel ratio

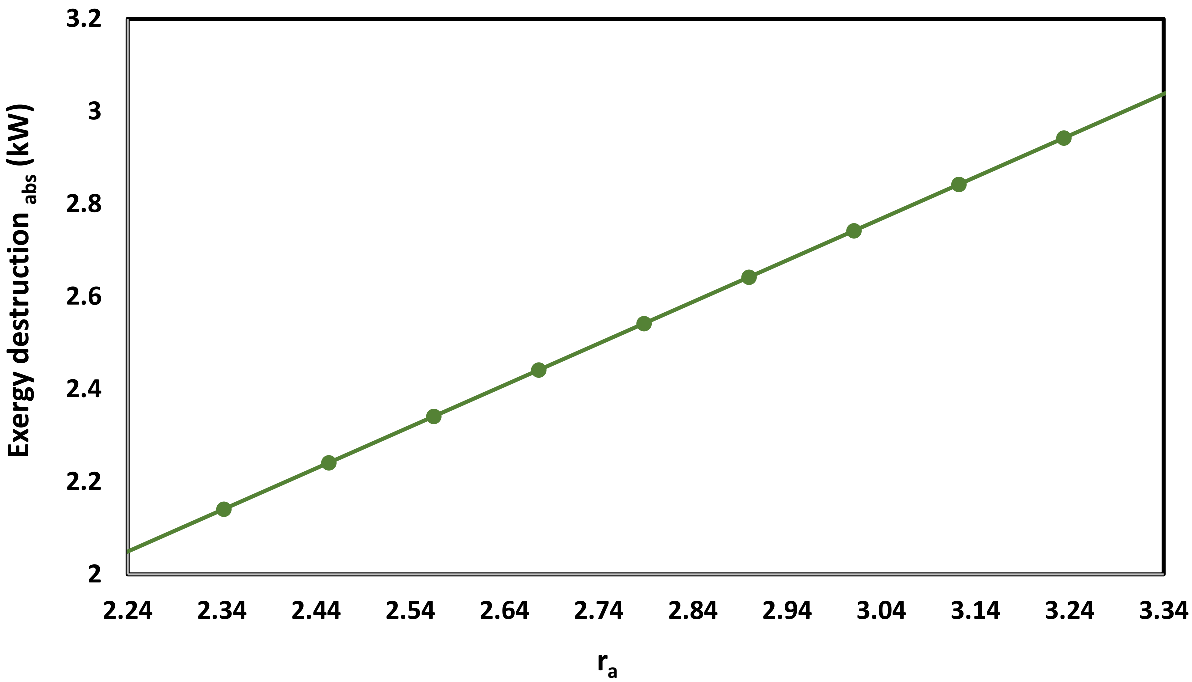

Figure 19. Variation of absorption chiller exergy destruction rate with air fuel ratio

Figure 20 presents the changes of systems energy and exergy efficiencies with variation of air fuel ratio. By increasing air fuel ratio, the temperature of exhaust gas is decreased too. The power production in Rankine cycle is decreased as a result. By increasing the power production in Rankine cycle, the system energy and exergy efficiencies are decreased, but this reduction is not considerable.

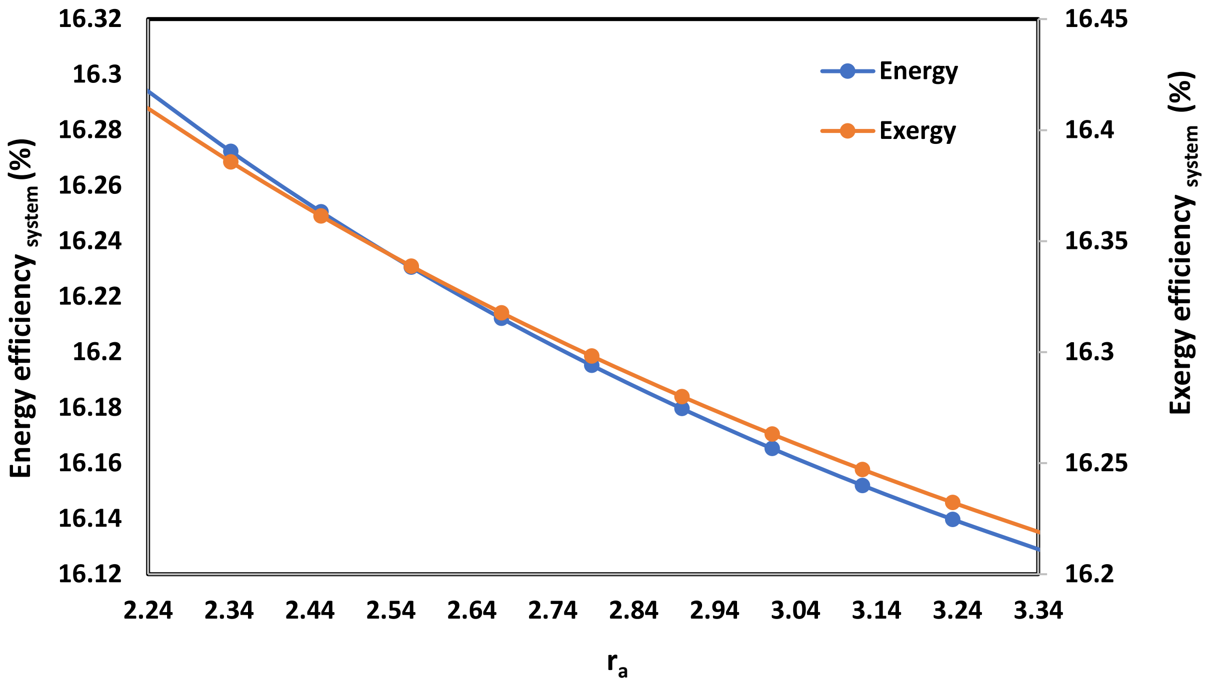

Figure 20. Variation of system energy and exergy efficiencies with air fuel ratio

4. Conclusion

In this study, the hybrid system powered by the coal combustion chamber and wind turbines is used to produce electricity, cooling load and syngas from the CO_2 emission of exhaust gas of the coal combustion chamber. The heat of exhaust gas of the combustion chamber runs a Rankine cycle for electricity generation and an absorption chiller to generate cooling load. The exhaust gas of the combustion chamber flows through a sulfur extraction unit to separate sulfur from CO_2. This CO_2 gas reacts with hydrogen (H_2) which is produced from water electrolysis process in an electrolyzer. The oxygen (O_2) generated from the water electrolysis process is injected into the combustion chamber to increase the efficiency of the combustion. The energy, exergy and economic analyses of this hybrid generation system have been performed.

The proposed system is capable of producing 1009.4 t of syngas annually and it can generate 180.5 MWh of cooling load and 40920.4 MWh of electricity. This configuration produces syngas while avoiding 2776 t of CO_2 emissions annually.

The maximum values of energy efficiency for compressor, methanation unit, steam power plant and wind turbine are about 85%, 83.5%, 30.1% and 30.7%. The maximum exergy efficiency for these components are 84.9%, 84.2%, 38.4% and 11.9%. In general, the energy and exergy efficiencies of this hybrid system are 16.6% and 16.2%. The production cost rates of electricity, cooling and syngas are 0.22, 0.074, and 0.12 $/kWh. The sensitivity analysis of this hybrid system relative to different parameters has been performed. The outcomes of this study can be summarized as follows:

By increasing the coal mass flow rate from 0.01 to 0.1 kg/s, the syngas production mass flow rate is increased from 0.08 to 0.89 kg/s. The electrical power of the electrolyzer is increased from 800 to 7900 kW.

By increasing the air-fuel ratio, the energy and exergy efficiencies of the burner are reduced due to increasing exergy destruction in this unit. Globally, the same situation is valid for energy, exergy and exergy destruction in the Rankine cycle, but the exergy destruction in the steam power plant is decreased slightly.

Based on economic investigation, the payback periods for this hybrid system with or without syngas production are 11.2 and 7.4 y. The IRR for the system with or without syngas production are 10 and 15%, and the NPV for this hybrid system are 1.6 and 8.45 US$.

The application of other renewable energies such as solar collector or geothermal energy instead of wind turbine can be used in association with this carbon capture and conversion system. This configuration can be employed for other hydrocarbon fuel combustion chamber to reduce CO_2 emissions as a future work on this topic.

Nomenclature

Subscript notations

0	Reference state condition (1atm, 288K)
1, 2, …, 15	Fifteen points in Figure 1
abs	Absorption chiller
act	Activation
Com	Compressor
C	Condenser
elec	Electrolyzer
E	Evaporator
FG	Flue gas
H	Hydrogen
ohm	Ohmic
O	Oxygen
P	Pump
rev	Reversible
S	Sulfur
T	Turbine

Variables

A	Area of electrode (m^2)
A_2	Swept area of wind turbine (m^2)
Abs	Absorption chiller

C	Parameter of wind turbine
C_0	Total investment cost (US$)
CF	Cost function ($)
COP	Coefficient of performance of absorption chiller
c_p	Specific heat at constant pressure (kJ/kgK)
ex	Total specific exergy (kJ/kg)
ex_{chi}	Component specific chemical exergy (kJ/kg)
$\dot{E}_D$	Exergy destruction rate
f_1 and f_2	Faraday efficiencies related to electrolyzer (mA^2/Cm^4)
F	Faraday`s constant (96495 C/mole)
h	Enthalpy (kJ/kg)
I	Current (A)
IRR	Internal Rate of Return
K	Parameter of wind turbine
K	Ratio (constant pressure divided to constant volume specific heat)
KK	Number of wind turbines
LHV	Lower heating value (kJ/kg)
$\dot{m}$	Mass flow rate (kg/s)
$\dot{m}_1$	$\dot{m}_{coal}$
$\dot{m}_{15}$	$\dot{m}_{\dot{O2},elec}$
$\dot{m}_2$	$\dot{m}_{air}$

$\dot{m}_3$	$\dot{m}_{FG}$
$\dot{m}_{H2}$	Hydrogen production mass flow rate in alkaline electrolyzer
N	Project lifetime equal to 25 years (y)
N_{cell}	Number of cells
NPV	Net Present Value (US$)
PP	Payback period (y)
$O2, elec$	Oxygen produced in the electrolyzer
P_{er}	Rated power of wind turbine (kW)
$\dot{Q}$	Heat transfer rate (kW)
r_1 and r_2	Ohmic resistance parameters (Ωm^2)
r_a	Air fuel ratio
r_c	Compressor pressure ratio
R	specific gas constant (kJ/kgK)
RC	Rankine cycle
R_i	Specific gas constant (kJ/kgK)
r	Discount factor equal to 3%
s	Specific entropy (kJ/kgK)
SPP	Simple Payback Period (y)
t_1, t_2 and t_3	electrode overvoltage coefficients (m^2/A)
T	Temperature (K)
T_1	T_{coal} (K)
T_{15}	$T_{O2,elec}$ (K)

T_2	T_{air} (K)
T_3	T_{FG} (K)
u	Wind velocity (m/s)
$\bar{u}$	Average wind speed (m/s)
u_c	Cut-in speed (m/s)
u_r	Rated speed (m/s)
u_f	Furling speed (m/s)
V	Operating voltage (V)
V_{cell}	Voltage of cells (V)
$\dot{W}$	Power transfer rate (kW)
$\dot{W}_c$	Consumption power in the compressor (kW)
$\dot{W}_{elec}$	Consumption power in alkaline electrolyzer (kW)
$\dot{W}_{wind,ave}$	Average electrical power generated by wind (kW) turbine
x	Weight fraction
x_1	x_{coal}
x_{15}	$x_{O2,elec}$
x_2	x_{air}
x_3	x_{FG}
σ	Standard deviation
ρ	Air density (kg/m^3)
η_C	Condenser heat transfer efficiency
η_E	Evaporator heat transfer efficiency

η_{CB}	Combustion loss efficiency
η_{Com}	Polytrophic compressor efficiency
η_{F}	Current efficiency of alkaline electrolyzer
η_{P}	Pump polythrophic efficiency
η_{T}	Turbine polythrophic efficiency
ΔG	Gibbs energy (equal to 237.2 kJ/mol)
Γ	Gamma function

Supplementary Information

In Figure S1, major steps of the method are illustrated as an overall diagram.

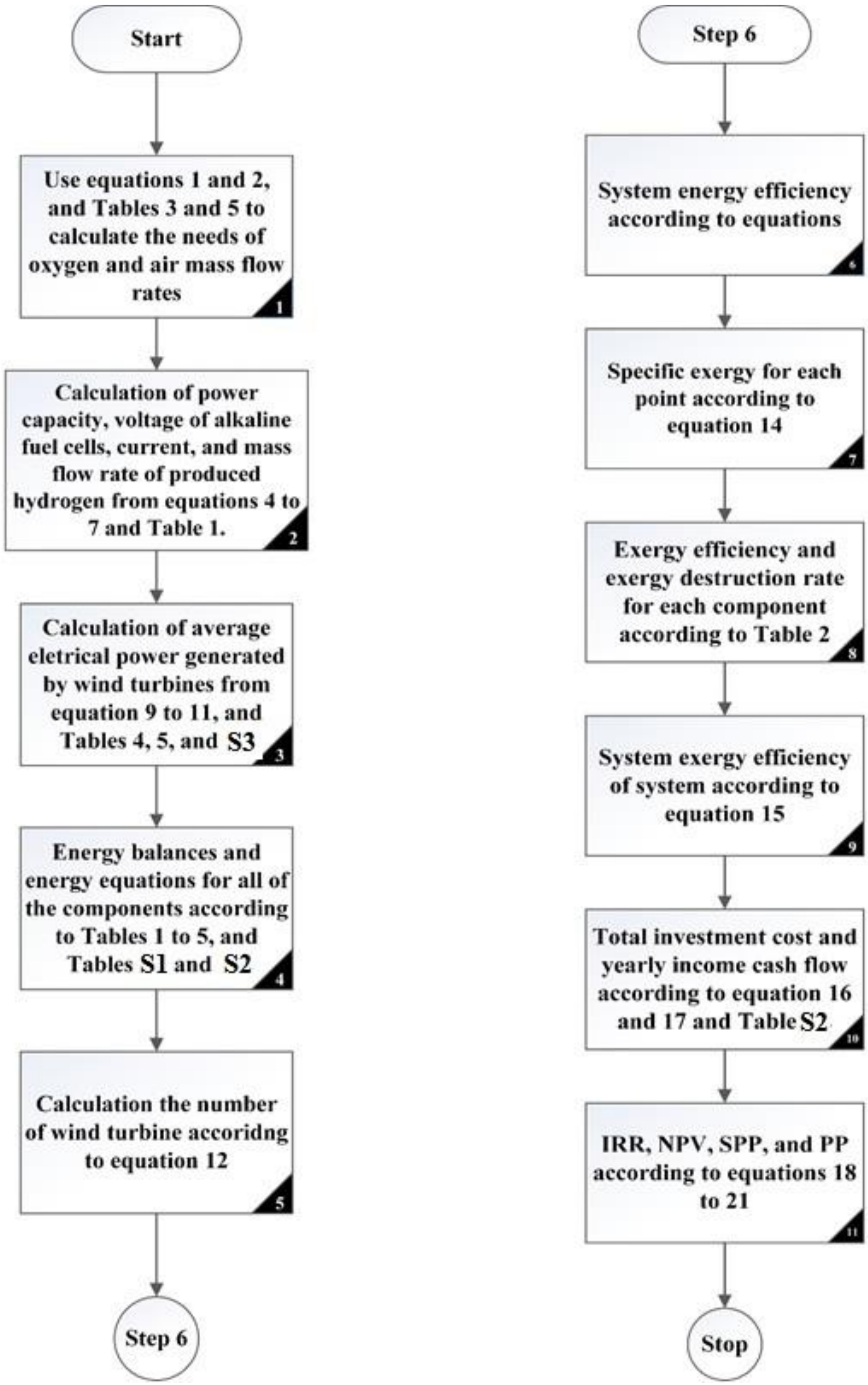

Figure S1. Overall diagram of major steps of the method

Energy and mass balances, and energy efficiency equation for each component of the system are listed in the Table S1.

Table S1. System component energy and mass balances as well as energy efficiency equations

No.	Component	Mass balance	Energy balance	Energy efficiency	References
1	**Burner**	$\dot{m}_{coal} + \dot{m}_{air} + \dot{m}_{coal} + \dot{m}_{O2,elec} = \dot{m}_{FG}$	$\eta_{cc}(\dot{m}_{coal} c_{p,coal}(T_{coal} - T_0) + \dot{m}_{air} c_{p,air}(T_{air} - T_0) + \dot{m}_{coal} LHV + \dot{m}_{O2,elec}\, c_{pO2,elec}(T_{O2,elec} - T_0)) = \dot{m}_{FG} c_{p,FG}(T_{FG} - T_0)$	$\frac{\dot{m}_3 c_{p,FG}\,(T_3 - T_0)}{\dot{m}_1 LHV_{coal}}$	(Bailera et al., 2015; Bejan, 2016; Cengel and Boles, 2002)
2	**Absorption chiller**	$\dot{m}_4 = \dot{m}_5$	$\dot{Q}_{abs} = COP \dot{m}_{FG} c_{p,FG}(T_4 - T_9)$	-	(Bejan, 2016; Cengel and Boles, 2002; Jawad Al-Tameemi et al., 2019)
3	**Pump**	$\dot{m}_8 = \dot{m}_5$	$\dot{W}_p = \frac{\dot{m}_{RC}(h_5 - h_8)}{\eta_p}$	$\frac{\dot{m}_{RC}(h_5 - h_8)}{\dot{W}_p}$	(Bejan, 2016; Cengel and Boles, 2002; Ehyaei and Rosen, 2019; Zeinodini and Aliehyaei, 2019)
4	**Evaporator**	$\dot{m}_6 = \dot{m}_5$ and $\dot{m}_4 = \dot{m}_3$	$\dot{Q}_E = \dot{m}_{RC}(h_6 - h_5) = \eta_E \dot{m}_{FG} C_{P_{FG}}(T_3 - T_4)$	$\frac{\dot{m}_{RC}(h_6 - h_5)}{\dot{m}_{RC}(h_6 - h_5)}$	(Bejan, 2016; Cengel and Boles, 2002; Ehyaei and Rosen, 2019; Zeinodini and Aliehyaei, 2019)
5	**Turbine**	$\dot{m}_6 = \dot{m}_7$	$\dot{W}_T = \dot{m}_{RC}(h_6 - h_7)\eta_T$	$\frac{\dot{W}_T}{\dot{m}_{RC}(h_6 - h_7)}$	(Bejan, 2016; Cengel and Boles, 2002; Ehyaei and Rosen, 2019; Zeinodini and Aliehyaei, 2019)
6	**Condenser**	$\dot{m}_8 = \dot{m}_7$	$\dot{Q}_C = \dot{m}_{RC}\eta_C(h_7 - h_8)$	$\frac{\dot{Q}_C}{\dot{m}_{RC}\,(h_7 - h_8)}$	(Bejan, 2016; Cengel and Boles, 2002; Ehyaei and Rosen, 2019; Zeinodini and Aliehyaei, 2019)
7	**Rankine cycle**	$\dot{m}_6 = \dot{m}_5 = \dot{m}_8 = \dot{m}_7$	-	$\frac{\dot{W}_T - \dot{W}_p}{\eta_E \dot{m}_{FG} C_{P_{FG}}(T_3 - T_4)}$	(Bejan, 2016; Cengel and Boles, 2002; Ehyaei and Rosen, 2019; Zeinodini and Aliehyaei, 2019)
8	**Alkaline electrolyzer**	$\dot{m}_{11} = \dot{m}_{12} + \dot{m}_{15}$	$\dot{m}_{11} h_{11} + \dot{W}_{elec} = \dot{m}_{12} h_{12} + \dot{m}_{15} h_{15}$	$\frac{\dot{m}_{12} LHV_{H_2}}{\dot{W}_{elec}}$	(Bejan, 2016; Cengel and Boles, 2002; Tijani et al., 2014; Ulleberg, 2003)

9	**Wind turbine**	-	$\dot{W}_{wind,ave} = \dot{W}_{wind,er}\left[\frac{\exp(-(\frac{u_c}{C}))^K - \exp(-(\frac{u_r}{C}))^K}{(\frac{u_r}{C})^K - (\frac{u_c}{C})^K} - \exp(-(\frac{u_f}{C}))^K\right]$	$\frac{\dot{W}_{windturbine,ave}}{\dot{W}_{windturbine,er}}$	(Asgari and Ehyaei, 2015; Ehyaei et al., 2019; Johnson, 2006; Justus, 1978; Powell, 1981)
10	**Methanation plant**	$\dot{m}_{10} + \dot{m}_{12} = \dot{m}_{13}$	$\dot{m}_{10}h_{10} + \dot{m}_{12}h_{12} = \dot{m}_{13}h_{13}$	$\frac{\dot{m}_{13}LHV_{CH_4}}{\dot{m}_{12}LHV_{H_2}}$	(Bailera et al., 2015; Cengel and Boles, 2002)
11	**Compressor**	$\dot{m}_{13} = \dot{m}_{14}$	$\dot{W}_{Com} = \dot{m}_{13}c_p\eta_{Com}(T_{14} - T_{13})$	$\frac{\dot{m}_{13}c_p(T_{14} - T_{13})}{\dot{W}_{Com}}$	(Cengel and Boles, 2002)

In Table S1, c_p is the specific heat at constant pressure, T is the temperature, $\dot{m}$ is the mass flow rate and LHV is the lower heating value. η_{CC} is the combustion efficiency which is equal to 85%, T_0 represents the ambient temperature which is 288.15 K (Yang et al., 2019; Yang et al., 2019). P, E, T, and C denote pump, evaporator, turbine and condenser. $\dot{W}$ and $\dot{Q}$ are power and heat transfer rate (kW). η is the polytrophic compressor efficiency.

According to Figure 1, $\dot{m}_{coal}$, T_{coal}, $\dot{m}_{air}$, T_{air}, $\dot{m}_{O2,elec}$, $T_{O2,elec}$, $\dot{m}_{FG}$ and T_{FG} are specified by $\dot{m}_1$, T_1, $\dot{m}_2$, T_2, $\dot{m}_{15}$, T_{15}, $\dot{m}_3$ and T_3. COP is the coefficient of performance of absorption chiller which is considered to be 0.85 (Waidhas et al., 1996).

Table S2. Exergy efficiency and exergy destruction rate equations for each component of the system

No.	Component	Exergy efficiency	Exergy destruction rate	References
1	**Burner**	$\frac{\dot{m}_3 ex_3}{\dot{m}_1 ex_1 + \dot{m}_2 ex_2 + \dot{m}_{15} ex_{15}}$	$\dot{m}_1 ex_1 + \dot{m}_{15} ex_{15} + \dot{m}_2 ex_2 - \dot{m}_3 ex_3$	(Bailera et al., 2015; Bejan, 2016; Cengel and Boles, 2002)
2	**Absorption chiller**	$\frac{\dot{Q}_{abs}\,(1 - \frac{T_0}{T_{abs}})}{\dot{m}_4(ex_4 - ex_9)}$	$\dot{m}_4(ex_4 - ex_9) - \dot{Q}_{abs}\,(1 - \frac{T_0}{T_{abs}})$	(Bejan, 2016; Cengel and Boles, 2002; Jawad Al-Tameemi et al., 2019)
3	**Pump**	$\frac{\dot{W}_p}{\dot{m}_{RC}(ex_8 - ex_5)}$	$\dot{m}_{RC}(ex_8 - ex_5) \mp \dot{W}_p$	(Bejan, 2016; Cengel and Boles, 2002; Ehyaei and Rosen, 2019; Zeinodini and Aliehyaei, 2019)
4	**Evaporator**	$\frac{\dot{m}_{RC}(ex_6 - ex_5)}{\dot{m}_{FG}(ex_3 - ex_4)}$	$\dot{m}_{RC} ex_5 + \dot{m}_{FG} ex_3 - \dot{m}_{Rc} ex_6 - \dot{m}_{FG} ex_4$	(Bejan, 2016; Cengel and Boles, 2002; Ehyaei and Rosen, 2019; Zeinodini and Aliehyaei, 2019)
5	**Turbine**	$\frac{\dot{W}_T}{\dot{m}_{RC}(ex_6 - ex_7)}$	$\dot{m}_{RC}(ex_6 - ex_7) - \dot{W}_T$	(Bejan, 2016; Cengel and Boles, 2002; Ehyaei and Rosen, 2019; Zeinodini and Aliehyaei, 2019)
6	**Condenser**	$\frac{\dot{Q}_{Con}(1 - \frac{T_0}{T_{Con}})}{\dot{m}_{RC}(ex_7 - ex_8)}$	$\dot{m}_{RC}(ex_7 - ex_8)$-$\dot{Q}_{Con}(1 - \frac{T_0}{T_C})$	(Bejan, 2016; Cengel and Boles, 2002; Ehyaei and Rosen, 2019; Zeinodini and Aliehyaei, 2019)
7	**Rankine cycle**	$\frac{\dot{W}_T - \dot{W}_p}{\dot{m}_{RC}(ex_6 - ex_5)}$	$\dot{Q}_E(1 - \frac{T_0}{T_E}) + \dot{W}_p - \dot{W}_T - \dot{Q}_{Con}(1 - \frac{T_0}{T_C})$	(Bejan, 2016; Cengel and Boles, 2002; Ehyaei and Rosen, 2019; Zeinodini and Aliehyaei, 2019)
8	**Alkaline electrolyzer**	$\frac{\dot{m}_{12} ex_{ch_{H_2}}}{\dot{W}_{elec}}$	$\dot{m}_{11} ex_{11} - \dot{m}_{15} ex_{15} - \dot{m}_{12} ex_{12} + \dot{W}_{elec}$	(Bejan, 2016; Cengel and Boles, 2002; Tijani et al., 2014; Ulleberg, 2003)
9	**Wind turbine**	$\frac{\dot{W}_{windturbine,ave}}{\frac{8}{27}\rho A_2 u^3}$	$\frac{8}{27}\rho A_2 u^3 - \dot{W}_{windturbine,ave}$	(Asgari and Ehyaei, 2015; Ehyaei et al., 2019; Johnson, 2006; Justus, 1978; Powell, 1981)

10	**Methanation plant**	$\frac{\dot{m}_{13}ex_{13}}{\dot{m}_{12}ex_{12}+\dot{m}_{10}ex_{10}}$	$\dot{m}_{12}ex_{12}+\dot{m}_{10}ex_{10}-\dot{m}_{13}ex_{13}$	(Bailera et al., 2015; Cengel and Boles, 2002)
11	**Compressor**	$\frac{\dot{W}_c}{\dot{m}_{13}ex_{13}-\dot{m}_{14}ex_{14}}$	$\dot{m}_{13}ex_{13}-\dot{m}_{14}ex_{14}+\dot{W}_{Com}$	(Cengel and Boles, 2002)

In Table S2, ρ denotes the density of air, A_2 defines the swept area of the wind turbine, u represents the wind velocity. $\dot{E}_D$ means the exergy destruction rate.

Installation and purchase cost of components are presented in the Table S3.

Table S3. Cost of purchase and installation of cycle components

Component	Cost function	Unit	References
Steam Cycle			
Turbine	$6000(\dot{W}_T)^{0.7}$	$	(Baghernejad and Yaghoubi, 2011; Owebor et al., 2019)
Pump	$3540(\dot{W}_P)^{0.71}$	$	(Baghernejad and Yaghoubi, 2011; Owebor et al., 2019)
Condenser	$1773\ \dot{m}_7$	$	(Baghernejad and Yaghoubi, 2011; Owebor et al., 2019)
Boiler	$1065900\ (0.001(\dot{W}_T-\dot{W}_P))^{0.8}$	$	(Caputo et al., 2005; Hasler et al., 2009; Kumar et al., 2015)
Civil work	$803860\ (0.001(\dot{W}_T-\dot{W}_P))^{0.5}$	$	(Caputo et al., 2005; Hasler et al., 2009; Kumar et al., 2015)
Electrical work	$835290\ (0.001(\dot{W}_T-\dot{W}_P))^{0.6}$	$	(Caputo et al., 2005; Hasler et al., 2009; Kumar et al., 2015)
Absorption chiller	$1144.3(\dot{Q}_{abs})^{0.67}$	$	(Dincer et al., 2017)
Wind turbine	1200000	$	(Powell, 1981)
Compressor	$\frac{39.5\dot{m}_{13}}{0.9-\eta_{Com}}(\frac{P_{14}}{P_{13}}\ln(\frac{P_{14}}{P_{13}}))$	$	(Baghernejad and Yaghoubi, 2011; Owebor et al., 2019)
Methanation	500	$/kW	(Baier et al., 2018)

Electrolyzer	1130	$/kW	(Baier et al., 2018)
CCS	$75.45 \cdot 10^6 (\frac{\dot{m}_{10}}{2.808 \cdot 10^6})^{0.65}$	$	(Bellotti et al., 2017)

For the Tehran city, wind velocity value for particular wind speed range are reported in the Table S4.

Table S4. Wind velocity value for particular wind speed range for Tehran

wind speed	Jan	Feb	Mar	Apr	May	Jun	Jul	Aug	Sep	Oct	Nov	Dec
$1 \leq u_1 < 3$	59	62	82	79	71	76	98	106	119	96	64	60
$4 \leq u_1 < 6$	25	36	65	61	53	67	73	51	43	37	31	8
$7 \leq u_1 < 10$	15	22	20	32	27	27	7	5	6	10	14	2
$11 \leq u_1 < 16$	0	2	2	7	12	3	2	1	0	2	2	2
$u_1 > 16$	0	0	0	0	0	0	0	0	0	0	0	0

References

Ahmadi, A., Jamali, D., Ehyaei, M.,Assad, M. E. H., 2020. Energy, Exergy, Economic and Exergoenvironmental analyses of gas and air bottoming cycles for production of electricity and hydrogen with gas reformer. Journal of Cleaner Production. 120915.

Anderson, B., 2015. Coal Fired Boiler-Principle 2. Seminar on Coal Fired Boiler, Malaysia.

Asgari, E.,Ehyaei, M. A., 2015. Exergy analysis and optimisation of a wind turbine using genetic and searching algorithms. International Journal of Exergy. 16(3), 293-314.

Atabi, F., Ehyaei, M. A.,Ahmadi, M. H. (2014). *Calculation of CH4 and CO2 emission rate in Kahrizak landfill site with LandGEM mathematical model.* Paper presented at the The 4th world sustainability forum.

Baghernejad, A.,Yaghoubi, M., 2011. Exergoeconomic analysis and optimization of an Integrated Solar Combined Cycle System (ISCCS) using genetic algorithm. Energy conversion and Management. 52(5), 2193-203.

Baier, J., Schneider, G.,Heel, A., 2018. A cost estimation for CO_2 reduction and reuse by methanation from cement industry sources in switzerland. Frontiers in Energy Research. 6, 5.

Bailera, M., Lisbona, P.,Romeo, L. M., 2015. Power to gas-oxyfuel boiler hybrid systems. International Journal of Hydrogen Energy. 40(32), 10168-75.

Bailera, M., Lisbona, P., Romeo, L. M.,Espatolero, S., 2016. Power to gas–biomass oxycombustion hybrid system: Energy integration and potential applications. Applied Energy. 167, 221-29.

Bejan, A., 2016. Advanced engineering thermodynamics. John Wiley & Sons, Hoboken, New Jersey.

Bellocchi, S., De Falco, M., Gambini, M., Manno, M., Stilo, T.,Vellini, M., 2019. Opportunities for power-to-gas and power-to-liquid in CO_2-reduced energy scenarios: The Italian case. Energy.

Bellos, E., Pavlovic, S., Stefanovic, V., Tzivanidis, C.,Nakomcic-Smaradgakis, B. B., 2019. Parametric analysis and yearly performance of a trigeneration system driven by solar-dish collectors. International Journal of Energy Research. 43(4), 1534-46.

Bellos, E., Tzivanidis, C.,Antonopoulos, K. A., 2016. Exergetic, energetic and financial evaluation of a solar driven absorption cooling system with various collector types. Applied Thermal Engineering. 102, 749-59.

Bellos, E., Tzivanidis, C., Symeou, C.,Antonopoulos, K. A., 2017. Energetic, exergetic and financial evaluation of a solar driven absorption chiller–A dynamic approach. Energy Conversion and Management. 137, 34-48.

Bellotti, D., Rivarolo, M., Magistri, L.,Massardo, A., 2017. Feasibility study of methanol production plant from hydrogen and captured carbon dioxide. Journal of CO_2 Utilization. 21, 132-38.

Boubenia, A., Hafaifa, A., Kouzou, A., Mohammedi, K.,Becherif, M., 2017. Carbone dioxide capture and utilization in gas turbine plants via the integration of power to gas. Petroleum. 3(1), 127-37.

Buttler, A.,Spliethoff, H., 2018. Current status of water electrolysis for energy storage, grid balancing and sector coupling via power-to-gas and power-to-liquids: A review. Renewable and Sustainable Energy Reviews. 82, 2440-54.

Caputo, A. C., Palumbo, M., Pelagagge, P. M.,Scacchia, F., 2005. Economics of biomass energy utilization in combustion and gasification plants: effects of logistic variables. Biomass and Bioenergy. 28(1), 35-51.

Castaneda, M., Cano, A., Jurado, F., Sánchez, H.,Fernandez, L. M., 2013. Sizing optimization, dynamic modeling and energy management strategies of a stand-alone PV/hydrogen/battery-based hybrid system. International Journal of Hydrogen Energy. 38(10), 3830-45.

Cengel, Y. A.,Boles, M. A., 2002. Thermodynamics: An engineering approach. Sea. 1000, 8862.

Conti, J., Holtberg, P., Diefenderfer, J., LaRose, A., Turnure, J. T.,Westfall, L. (2016). International energy outlook 2016 with projections to 2040: USDOE Energy Information Administration (EIA), Washington, DC (United States ….

De Santoli, L., Basso, G. L.,Nastasi, B., 2017. The potential of hydrogen enriched natural gas deriving from power-to-gas option in building energy retrofitting. Energy and Buildings. 149, 424-36.

Dincer, I., Rosen, M. A.,Ahmadi, P., 2017. Optimization of energy systems. Wiley Online Library, New York.

Dorotić, H., Doračić, B., Dobravec, V., Pukšec, T., Krajačić, G.,Duić, N., 2019. Integration of transport and energy sectors in island communities with 100% intermittent renewable energy sources. Renewable and Sustainable Energy Reviews. 99, 109-24.

Ehyaei, M. A., Ahmadi, A.,Rosen, M. A., 2019. Energy, exergy, economic and advanced and extended exergy analyses of a wind turbine. Energy Conversion and Management. 183, 369-81.

Ehyaei, M. A.,Rosen, M. A., 2019. Optimization of a triple cycle based on a solid oxide fuel cell and gas and steam cycles with a multiobjective genetic algorithm and energy, exergy and economic analyses. Energy Conversion and Management. 180, 689-708.

García–García, I., Barrio, V.,Cambra, J., 2018. Power-to-gas: Storing surplus electrical energy. Study of catalyst synthesis and operating conditions. International Journal of Hydrogen Energy. 43(37), 17737-47.

Ghaib, K.,Ben-Fares, F.-Z., 2018. Power-to-methane: A state-of-the-art review. Renewable and Sustainable Energy Reviews. 81, 433-46.

Gholizadeh, N., Vahid-Pakdel, M.,Mohammadi-ivatloo, B., 2019. Enhancement of demand supply's security using power to gas technology in networked energy hubs. International Journal of Electrical Power & Energy Systems. 109, 83-94.

Gondal, I. A., 2019. Hydrogen integration in power-to-gas networks. International Journal of Hydrogen Energy. 44(3), 1803-15.

Guandalini, G., Robinius, M., Grube, T., Campanari, S.,Stolten, D., 2017. Long-term power-to-gas potential from wind and solar power: A country analysis for Italy. International Journal of Hydrogen Energy. 42(19), 13389-406.

Hasler, D., Rosenquist, W.,Gaikwad, R., 2009. New coal-fired power plant performance and cost estimates. Sargent and Lundy project. 1-82.

Iaquaniello, G., Setini, S., Salladini, A.,De Falco, M., 2018. CO_2 valorization through direct methanation of flue gas and renewable hydrogen: A technical and economic assessment. International Journal of Hydrogen Energy. 43(36), 17069-81.

Jamali, D. H.,Noorpoor, A., 2019. Optimization of a novel solar-based multi-generation system for waste heat recovery in a cement plant. Journal of Cleaner Production. 240, 117825.

Jawad Al-Tameemi, M. R., Liang, Y.,Yu, Z., 2019. Combined ORC-HP thermodynamic cycles for DC cooling and waste heat recovery for central heating. Energy Procedia. 158, 2046-51.

Johnson, G. L., 2006. Wind energy systems. Citeseer, Prentice Hall, Englewood Cliffs, NJ.

Justus, C. G., 1978. Winds and wind system performance. Research supported by the National Science Foundation and Energy Research and Development Administration. Philadelphia, Pa., Franklin Institute Press, 1978. 120 p.

Kirchbacher, F., Biegger, P., Miltner, M., Lehner, M.,Harasek, M., 2018. A new methanation and membrane based power-to-gas process for the direct integration of raw biogas–Feasability and comparison. Energy. 146, 34-46.

Kreuter, W.,Hofmann, H., 1998. Electrolysis: the important energy transformer in a world of sustainable energy. International Journal of Hydrogen Energy. 23(8), 661-66.

Kumar, R., Sharma, A. K.,Tewari, P., 2015. Cost analysis of a coal-fired power plant using the NPV method. Journal of Industrial Engineering International. 11(4), 495-504.

Lewandowska-Bernat, A.,Desideri, U., 2018. Opportunities of power-to-gas technology in different energy systems architectures. Applied Energy. 228, 57-67.

Li, Z. X., Ehyaei, M. A., Kamran Kasmaei, H., Ahmadi, A.,Costa, V., 2019. Thermodynamic modeling of a novel solar powered quad generation system to meet electrical and thermal loads of residential building and syngas production. Energy Conversion and Management. 199, 111982.

Lisbona, P., Frate, G. F., Bailera, M.,Desideri, U., 2018. Power-to-gas: Analysis of potential decarbonization of Spanish electrical system in long-term prospective. Energy. 159, 656-68.

Llera, E., Romeo, L., Bailera, M., Osorio, J., Ebro, C. R.,de Luna, M., 2018. Exploring the integration of the power to gas technologies and the sustainable transport. Towards Energy Sustain. 77.

Miao, B.,Chan, S. H., 2019. The economic feasibility study of a 100-MW power-to-gas plant. International Journal of Hydrogen Energy.

Mozafari, A.,Ehyaei, M. A., 2012. Effects of Regeneration Heat Exchanger on Entropy, Electricity Cost, and Environmental Pollution Produced by Micro Gas Turbine System. International Journal of Green Energy. 9(1), 51-70.

Nakomčić-smaragdakis, B. B.,Dragutinović, N. G., 2016. Hybrid renewable energy system application for electricity and heat supply of a residential building. Thermal Science. 20(2).

Owebor, K., Oko, C., Diemuodeke, E.,Ogorure, O., 2019. Thermo-environmental and economic analysis of an integrated municipal waste-to-energy solid oxide fuel cell, gas-, steam-, organic fluid-and absorption refrigeration cycle thermal power plants. Applied energy. 239, 1385-401.

Pierrot, M., 2019. The wind power database. See www.thewindpower.net.

Powell, W. R., 1981. An analytical expression for the average output power of a wind machine. Solar Energy. 26(1), 77-80.

Roadmap, E. (2011). Mapping renewable energy pathways towards 2020: EREC.

Schaaf, T., Grünig, J., Schuster, M. R., Rothenfluh, T.,Orth, A., 2014. Methanation of CO_2-storage of renewable energy in a gas distribution system. Energy, Sustainability and Society. 4(1), 2.

Shaygan, M., Ehyaei, M. A., Ahmadi, A., Assad, M. E. H.,Silveira, J. L., 2019. Energy, exergy, advanced exergy and economic analyses of hybrid polymer electrolyte membrane (PEM) fuel cell and photovoltaic cells to produce hydrogen and electricity. Journal of Cleaner Production. 234, 1082-93.

Shirmohammadi, R., Soltanieh, M.,Romeo, L. M., 2018. Thermoeconomic analysis and optimization of post-combustion CO_2 recovery unit utilizing absorption refrigeration system for a natural-gas-fired power plant. Environmental Progress & Sustainable Energy. 37(3), 1075-84.

Suresh, M., Reddy, K.,Kolar, A., 2012. Thermodynamic analysis of a coal-fired power plant repowered with pressurized pulverized coal combustion. Proceedings of the Institution of Mechanical Engineers, Part A: Journal of Power and Energy. 226(1), 5-16.

Thema, M., Bauer, F.,Sterner, M., 2019. Power-to-gas: Electrolysis and methanation status review. Renewable and Sustainable Energy Reviews. 112, 775-87.

Tijani, A. S., Yusup, N. A. B.,Rahim, A. H. A., 2014. Mathematical modelling and simulation analysis of advanced alkaline electrolyzer system for hydrogen production. Procedia Technology. 15, 798-806.

Toro, C.,Sciubba, E., 2018. Sabatier based power-to-gas system: Heat exchange network design and thermoeconomic analysis. Applied energy. 229, 1181-90.

Tzivanidis, C., Bellos, E.,Antonopoulos, K. A., 2016. Energetic and financial investigation of a stand-alone solar-thermal Organic Rankine Cycle power plant. Energy conversion and management. 126, 421-33.

Ulleberg, Ø., 2003. Modeling of advanced alkaline electrolyzers: a system simulation approach. International Journal of Hydrogen Energy. 28(1), 21-33.

Verma, A., Singh, T.,Monjezi, M., 2010. Intelligent prediction of heating value of coal. Iranian Journal of Earth Sciences. 2, 32-38.

Waidhas, M., Drenckhahn, W., Preidel, W.,Landes, H., 1996. Direct-fuelled fuel cells. Journal of Power Sources. 61(1), 91-97.

Walker, S. B., van Lanen, D., Mukherjee, U.,Fowler, M., 2017. Greenhouse gas emissions reductions from applications of Power-to-Gas in power generation. Sustainable Energy Technologies and Assessments. 20, 25-32.

Weidner, S., Faltenbacher, M., François, I., Thomas, D., Skùlason, J.,Maggi, C., 2018. Feasibility study of large scale hydrogen power-to-gas applications and cost of the systems evolving with scaling up in Germany, Belgium and Iceland. International Journal of Hydrogen Energy. 43(33), 15625-38.

Wulf, C., Linßen, J.,Zapp, P., 2018. Review of power-to-gas projects in Europe. Energy Procedia. 155, 367-78.

Yang, A., Jin, S., Shen, W., Cui, P., Chien, I. L.,Ren, J., 2019. Investigation of energy-saving azeotropic dividing wall column to achieve cleaner production via heat exchanger network and heat pump technique. Journal of Cleaner Production. 234, 410-22.

Yang, A., Su, Y., Chien, I. L., Jin, S., Yan, C., Wei, S. a.,Shen, W., 2019. Investigation of an energy-saving double-thermally coupled extractive distillation for separating ternary system benzene/toluene/cyclohexane. Energy. 186, 115756.

Yang, Y., Guo, S., Liu, D., Li, R.,Chu, Y., 2018. Operation optimization strategy for wind-concentrated solar power hybrid power generation system. Energy Conversion and Management. 160, 243-50.

Zeinodini, M.,Aliehyaei, M., 2019. Energy, exergy, and economic analysis of a new triple-cycle power generation configuration and selection of the optimal working fluid. Mechanics & Industry. 20(5).